Accepted Manuscript

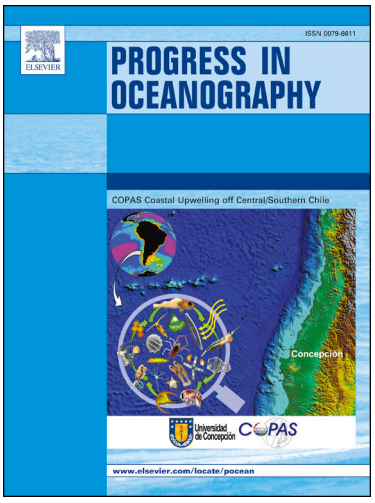

Sedimentary processes and cold-water coral mini-mounds at the Ferrol canyon head, NW Iberian margin

Tim Collart, Wencke Verreydt, F. Javier Hernández-Molina, Estefanía Llave, Ricardo León, María Gómez-Ballesteros, Edwige Pons-Branchu, Heather Stewart, David Van Rooij

PII: S0079-6611(17)30241-0
DOI: https://doi.org/10.1016/j.pocean.2018.02.027
Reference: PROOCE 1931

To appear in: *Progress in Oceanography*

Please cite this article as: Collart, T., Verreydt, W., Javier Hernández-Molina, F., Llave, E., León, R., Gómez-Ballesteros, M., Pons-Branchu, E., Stewart, H., Van Rooij, D., Sedimentary processes and cold-water coral mini-mounds at the Ferrol canyon head, NW Iberian margin, *Progress in Oceanography* (2018), doi: https://doi.org/10.1016/j.pocean.2018.02.027

Sedimentary processes and cold-water coral mini-mounds at the Ferrol canyon head, NW Iberian margin

Tim COLLART[1,*], Wencke VERREYDT[1], F. Javier HERNÁNDEZ-MOLINA[2], Estefanía LLAVE[3], Ricardo LEÓN[3], María GÓMEZ-BALLESTEROS[4], Edwige PONS-BRANCHU[5], Heather STEWART[6] and David VAN ROOIJ[1]

[1] Department of Geology, Ghent University, Krijgslaan 281 S8, 9000 Ghent, Belgium (tim.collart@ugent.be)

[2] Department of Earth Sciences, Royal Holloway, University of London, Egham, Surrey TW20 0EX, UK

[3] Instituto Geológico y Minero de España, Ríos Rosa 23, 28003 Madrid, Spain

[4] Instituto Español de Oceanografía, Corazón de María 8, 28002 Madrid, Spain

[5] Laboratoire des Sciences du Climat et de l'Environnement, LSCE/IPSL, CEA-CNRS-UVSQ, Université Paris-Saclay, F-91191 Gif-sur-Yvette, France

[6] British Geological Survey (BGS), Lyell Centre, Research Ave S, Edinburgh EH14 4AP, UK

Abstract :

The western Iberian margin has a complex morphology controlled by both geological and oceanographic processes. Compared to the submarine canyons in the southern part of this margin (e.g. Nazaré and Setubal), the canyons in the northern part (e.g. Ferrol and A Coruña) have received little attention. This study maps the geomorphological features around the Ferrol canyon head and combines them with oceanographic observations to infer the sedimentary and oceanographic processes active in this area. Furthermore, the occurrence of a cold-water coral (CWC) mini-mound province near the canyon head and the Ortegal Spur pockmark field is investigated with regard to seepage processes, oceanographic conditions and anthropogenic impact.

The Ferrol canyon head and outer Ortegal Spur are characterized by erosional (erosional and abraded surfaces, contourite channels and furrows), depositional (contourite drifts and sediment waves) and mixed (contourite terrace) features, indicating a dominant control of bottom currents on the sedimentary processes. Bottom currents are related to the interaction of the canyon head topography with both the Mediterranean Outflow Water (MOW) slope current and with M2 internal tides associated to the interface

* Corresponding author.

(pycnocline) between Eastern North Atlantic Central Water (ENACW) and MOW. Due to this interaction, the Ferrol canyon head is subject to active sediment resuspension and forms a potential source area for the intermediate nepheloid layers along the NW Iberian upper slope.

The CWC mini-mounds (1.9-2.7 m high and 75-141 m in diameter) occur between 400-560 m depth. Seismic facies signatures indicative of fluid-flow and morphometric analysis implies that larger CWC mini-mounds adjacent to the pockmark field initiated by colonization of pre-existing pockmarks, while smaller more clustered mounds developed independently. The observed mini-mounds are relict features likely related to their position outside of the contemporary ENACW-MOW interface which favours CWC growth through (1) increased bottom currents, enhancing food supply and (2) the presence of a potential density envelope σ_θ = 27.35-27.65 kg/m^3, proposed to control coral larvae transport along the NE Atlantic margin. Alternatively, the lack of contemporary coral growth might be related to habitat destruction by bottom trawling. However, a preliminary age constraint reveals CWC growth occurred during the early Holocene, coeval to relict CWC mini-mounds near canyon heads on the Armorican margin. Their existence suggests a regional shift in the NE Atlantic density profile where the ENACW-MOW interface occurred up to 200 m above its contemporary position.

Keywords: submarine canyon processes, bottom currents, Mediterranean Outflow Water, internal tides, cold-water corals, pockmarks, NW Iberian margin

1. Introduction

Submarine canyons provide the main pathway for sediment transport between the shelf and the deep ocean by turbidity currents, hyperpycnal flows, slope failures, dense shelf water cascading or by focusing of internal waves, causing resuspension and creating bottom nepheloid layers (BNLs) and intermediate nepheloid layers (INLs; e.g. Allen & Durrieu de Madron, 2009; Puig et al., 2014). On the western Iberian margin, major canyons that intersect the entire continental slope are only found in the southern sector (e.g. Nazaré and Setubal) where they intercept sediment transport across the shelf and upper slope and provide a direct conduit to the deep ocean (de Stigter et al., 2007; Oliveira et al., 2007; Arzola et al., 2008). In contrast, the canyons in the northern sector (e.g. Ferrol Canyon and A Coruña), do not reach the shelf but rather incise a series of marginal platforms on the upper slope (Maestro et al., 2013). Their role in

contemporary sediment transport has not been reported in literature. Along the NW Iberian margin, water column turbidity studies have indicated that modern sediment delivery to the deeper ocean is mainly derived from primary production in the surface nepheloid layer (SNL) and by settling from INLs (Hall et al., 2000; McCave & Hall, 2002; van Weering et al., 2002). A shallow INL occurs at 100-300 m water depth as a result of shelf edge resuspension and off-shelf transport (McCave & Hall, 2002). A deeper INL at 500-800 m results from resuspension by the interaction of the upper slope topography with the northward flowing Mediterranean Outflow Water (MOW) and/or internal waves and tides associated with the pycnocline at the interface between the Eastern North Atlantic Central Water (ENACW) and the MOW (McCave & Hall, 2002). The importance of this process is illustrated by the sediment distribution on the NW Iberian margin. The lower slope is dominated by calcareous muds while the upper slope is characterized by an increased terrigenous content with coarser grainsize or even rocky outcrops indicating the absence of modern sediments (Flach et al., 2002; van Weering et al., 2002). The MOW slope current also plays an important role in the along-slope redistribution of sediment as evidenced by the presence of several large contourite depositional systems (CDS) along the Iberian margin (Hernández-Molina et al., 2011; Hanebuth et al., 2015; Llave et al., 2015). In particular, the Ferrol and A Coruña submarine canyons are influenced by the Ortegal CDS (Hernández-Molina et al., 2011; Maestro et al., 2013; Llave et al., 2015; Hernández-Molina et al., 2016)

A new province of cold-water coral (CWC) mini-mounds was described around the Ferrol canyon head (Hernández-Molina et al., 2010) and adjacent to the Ortegal Spur pockmark field (Jané et al., 2010). CWC mounds are constructed by framework building scleractinian corals like *Lophelia pertusa* and *Madrepora oculata* that have the ability to baffle sediment and over time, develop carbonate mounds (Freiwald et al., 2004; Roberts et al., 2006). Historically, CWC's were thought to rely on hydrocarbon seepage for their food supply, based on their reported co-occurrence with seepage related structures (Hovland & Thomsen, 1997; Henriet et al., 1998; Henriet et al.; Hovland & Risk, 2003; Hovland, 2005). However, the isotopic carbon signature of coral tissue and skeleton excludes a seepage-based food chain and indicates food particles are derived from surface primary productivity (Duineveld et al., 2004; Kiriakoulakis et al., 2005; Duineveld et al., 2007). Instead, the co-occurrence is likely related to methane-derived authigenic carbonates formed in seepage sites (Friedman et al., 1988; Hovland & Judd, 1988; Boetius et al., 2000;

Greinert et al., 2001; Magalhães et al., 2012) which offer suitable hard grounds for coral colonisation (Kellogg et al., 2009; Wehrmann et al., 2011; Magalhães et al., 2012; Somoza et al., 2014).

Along the NE Atlantic margin, CWC provinces predominantly fall within a narrow depth range (500-1000 m) characterized by the permanent thermocline (White & Dorschel, 2010). Vigorous bottom currents, resulting from the interaction between the steep continental slope and internal motions associated with the steep vertical density gradient at this water depth interval, are thought to create favourable conditions for CWC mound development (White & Dorschel, 2010; Mohn et al., 2014; van Haren et al., 2014). The filter-feeding corals benefit from this dynamic environment as it enhances the delivery of food particles to their polyps while preventing the corals from being smothered by fine sediment (White et al., 2005; Duineveld et al., 2007; Mienis et al., 2007; White, 2007). This hydrodynamic regime also influences sedimentary processes and CWC mounds are often found in association with INLs and BNLs (Mienis et al., 2007; White & Dorschel, 2010; Huvenne et al., 2011) and contourite related features (Huvenne et al., 2009b; Van Rooij et al., 2009; Hebbeln et al., 2016). Furthermore, the potential density envelope σ_θ = 27.35-27.65 kg/m^3 present at permanent thermocline depth seems to exert some control over the distribution of live *L. pertusa* along the NE Atlantic margin and it has been hypothesised to govern coral larvae transport (Dullo et al., 2008; Flögel et al., 2014; Rüggeberg et al., 2016). Interestingly, the CWC mini-mound province at the Ferrol canyon head, as well as provinces of similarly sized mound at the head of submarine canyons on the Celtic (Stewart et al., 2014), Armorican (De Mol et al., 2011) and Cantabrian (Sánchez et al., 2014) margins occur at shallower (250-500 m) water depth, above the permanent thermocline. These provinces appear devoid of modern coral growth but as of yet, it is unknown if this is caused solely by a change to unfavourable environmental conditions or by bottom trawling activity destroying the reef habitat (De Mol et al., 2011; Sánchez et al., 2014; Stewart et al., 2014).

This work describes the geomorphological features and the oceanography of the Ferrol canyon head and the outer Ortegal spur with the aim to: (1) document and explain the interactions between the sedimentary and oceanographic processes active in and around the canyon head; (2) characterize the CWC mini-mounds and examine the relationship between coral occurrence and seepage processes, oceanographic conditions and anthropogenic impact. Finally, (3) the palaeoceanographic implications of this mini-mound province are briefly discussed.

2. Regional setting

The study area lies approximately 30 km off the coast of Cabo Ortegal, at the NW corner of the Iberian Peninsula between 200-1030 m depth. It is located on the western part of the Ortegal Spur, a marginal platform on the upper continental slope of the NW Iberian margin (Fig. 1a). The western part of the platform is deeply incised by the head of the Ferrol and A Coruña submarine canyons.

2.1 Geological setting

The Ortegal Spur originated from a continental-rifting phase related to the opening of the Atlantic domain during the Late Jurassic through Early Cretaceous (Williams, 1975; Knott et al., 1993). By the Late Cretaceous it had gradually changed into a passive margin with the onset of oceanic crust formation in the Bay of Biscay (Boillot et al., 1987). In the Early Cenozoic, a convergence between the Eurasian and Iberian plate provoked a reactivation of the rift structures and a partial southward subduction of the Bay of Biscay seafloor beneath the Iberian margin. This resulted in inversion of normal faults causing tectonic deformation of the Mesozoic basement and the overlying upper Eocene limestone during the Eocene and emergence of the margin during the Oligocene (Boillot et al., 1979). In the late Paleogene and Neogene the northern Iberian margin was again submerged (Boillot et al., 1979) coeval with an active subsidence stage and Neogene sediments were deposited in a relatively deep depositional environment (Boillot et al., 1987). The overlying Pliocene to Quaternary deposits have an irregular distribution and were deposited on a glacially influenced margin (Weaver et al., 2000; Mojtahid et al., 2005) where sediment transfer mainly took place downslope through submarine canyons (Bourillet et al., 2006; Gaudin et al., 2006; Gonthier et al., 2006). Locally, bottom current processes play an important role in shaping the margin but their occurrence is controlled by glacio-eustatic sea level changes (Ercilla et al., 2008; Hernández-Molina et al., 2011; Maestro et al., 2013; Llave et al., 2015; Hernández-Molina et al., 2016).

2.2 Oceanographic setting

Two different water masses are present in the study area: the Eastern North Atlantic Central Water (ENACW) the Mediterranean Outflow Water (MOW; Pollard et al., 1996; Fiúza et al., 1998; Van Aken, 2000). The ENACW forms the upper water mass and is subdivided in the subtropical ENACWst ($\Theta \geq 12.2°$ C, S ≥ 35.66; Harvey, 1982) situated between 100-400 m depth, and the subpolar ENACWsp ($\Theta \geq 8.56°$ C, S ≥ 35.23; Castro et al., 1998) between 400-700 m depth (Fiúza et al., 1998). During the summer upwelling

season (April to September), the ENACWsp flows equatorward in the relatively weak Portugal Current (PC) and Portugal Coastal Current (PCC) and a subsurface front develops between the two modes of ENACW located off the coast of Cape Finisterre (Fig. 1b; Finisterre Front; Varela et al., 2005). During winter downwelling (October to March), the Iberian Poleward Current system (IPCs) develops, transporting ENACWst over the shelf and slope (Fig. 1b), displacing the front northward (Castro et al., 1998; Peliz et al., 2005; Varela et al., 2005). The MOW is present between 600-1400 m depth and is characterized by high salinity ($S \geq 36.0$) and relatively high potential temperature ($\Theta \approx 11°$ C; Daniault et al., 1994; Fiúza et al., 1998; Iorga & Lozier, 1999a; Van Aken, 2000). It flows along the continental slope as a density driven slope current, conditioned by the Coriolis force and seafloor irregularities (Pingree & Le Cann, 1990; Diaz del Rio et al., 1998; Hernández-Molina et al., 2011). Along its path, its characteristic salinity decreases due to mixing with the surrounding water masses (Diaz del Rio et al., 1998; Iorga & Lozier, 1999a). Around the Galicia Bank, the MOW is thought to split up into two branches with one flowing west of the bank and the other, more saline one, flowing north along the Iberian continental slope (Fig. 1b). After reaching the study area, this branch turns to the east into the Bay of Biscay (Mazé et al., 1997; Iorga & Lozier, 1999a). During summer upwelling, the MOW core is more tightly attached to the continental slope (Prieto et al., 2013) and is displaced upward-inshore through Ekman pumping (García Lafuente et al., 2008). In winter, the situation reverses, the MOW spreads out to the open ocean and flow reversals towards the equator occur (Friocourt et al., 2007; 2008; Prieto et al., 2013). The strong pycnocline at the interface between the ENACW and MOW (Fiúza et al., 1998) gives rise to baroclinic motions. Several authors have reported the generation of freely propagating internal tides with dominant semi-diurnal M2 frequency by the interaction of the barotropic tides with the NW Iberian slope (Azevedo et al., 2006; García-Lafuente et al., 2006; Pichon et al., 2013). At its lower boundary the MOW is influenced by mixing with the relatively cold ($\Theta \approx 3.5°$ C) and fresh ($S \approx 34.89$) Labrador Sea Water (LSW) which is present outside the study area at 1500 - 2000 m depth (Talley & McCartney, 1982; Fiúza et al., 1998).

3. Material and methods

The high-resolution seismic reflection profiles, swath bathymetry and backscatter intensity, oceanographic data, Remotely Operated underwater Vehicle (ROV) observations and coral sample used in this study, were acquired during three consecutive legs of R/V Belgica cruise 09/14 in May-June 2009.

3.1 Seismic reflection profiling

The high-resolution 2D single channel seismic reflection data (Fig. 2) were collected using a SIG sparker source (120 electrodes), a single channel surface streamer and Delph acquisition software. The trigger interval was set at 2 s, energy output at 500 J, sampling frequency at 8 kHz and record length at 1900 ms two-way travel time (TWT). At greater water depths, the trigger interval was adjusted to 3 s and the record length was increased to 2900 ms TWT. The vessel velocity was kept at 4 knots using electrical propulsion for noise reduction. The seismic data was processed in RadExPro 2013.1 with a bandpass (Butterworth, low pass of 1500 Hz and high pass of 200 Hz), a swell and a burst noise removal filter as well as a spherical divergence amplitude correction. Visualization and interpretation was conducted with the KINGDOM suite 8.8 software.

3.2 Multibeam echosounder

The multibeam swath bathymetry (Fig. 2) and backscatter data (Fig. 3a) was collected with the shipboard Simrad EM1002 multibeam echosounder. The beam angle was set at 70° and average survey water depth at 750 m, keeping a 10-20 % overlap between swaths. The vessel velocity was kept between 5 and 8 knots. The data was processed with IFREMER CARAIBES software release 3.4 and visualized using Fledermaus 6.7.0k Professional software and ESRI Arcmap 10.1. The bathymetric and backscatter data was gridded at a cell size of both 5 and 15 m. This data was combined with the seismic reflections profiles to construct a geomorphological map (Fig. 3b). The morphological features were classified according to literature (Hovland & Judd, 1988; Faugères et al., 1999; Rebesco & Camerlenghi, 2008; Stow et al., 2009; Rebesco et al., 2014) and grouped based on their origin into tectonic, erosional, depositional, mixed (erosional and depositional), mass wasting, fluid migration and biogenic features (Fig. 3b).

The mini-mounds and pockmarks were mapped using the BGS Arcmap semi-automated feature mapping tool (Gafeira et al., 2015; De Clippele et al., 2016) based on a Bathymetric Positional Index (BPI) grid. BPI is a measure for the positioning of a reference location to the neighbouring locations. Positive BPI values indicate elevated regions, negative BPI indicate depressions and low to zero BPI indicate either flat areas or areas with constant slope. The analysis neighbourhood is scalable which allows to fine-tune the BPI grid to highlight small scale variations in the bathymetry (Weiss, 2001). Fine scale BPI grids were constructed from the 5 m resolution bathymetric grid using the Benthic Terrain Modeller extension

(Wright et al., 2012). The analysis neighbourhood was defined as an annulus with an inner radius of 25 grid cells (125 m) and outer radius of 50 grid cells (250 m). The threshold BPI and minimum feature BPI were both set to 1 for mounds and -1 for pockmarks. A minimum feature area of 100 m^2 was set to prevent processing artefacts being mapped and a minimum width to length ratio of 0.1 was used to prevent elongated bathymetric features (e.g. ridges) from being mapped (Gafeira et al., 2015). Due to an error in sound velocity, part of the swath overlaps display a relict relief of up to 2 m, obscuring parts of the pockmarks and mini-mounds. This introduced errors in the feature outlines determined by the mapping tool and required manual editing. From the mapped feature outlines, morphological characteristics were measured. Subsequently, a morphometric approach was used to assess a potential genetic link between the pockmarks and mini-mounds. The identified features were divided into 3 groups: (1) pockmarks, (2) southern mini-mounds located to the southeast of the Ferrol canyon head, adjacent to the pockmark field and (3) northern mini-mounds located to the north of the Ferrol canyon head. Only morphological characteristics that would be preserved in the evolution from pockmarks to mini-mound were used in the analysis: mean diameter (mean of the width and length), width to length ratio, azimuth of the long axis and distance to the nearest neighbouring feature. These characteristics were then analysed using a non-parametric multivariate statistical approach using R version 3.2.3. (RCoreTeam, 2015) with the vegan package (Jari et al., 2017). Principal Component Analysis (PCA; Davis, 1986) was performed on the standardized characteristics to visually assess differences between the different groups. One-way Permutational Multivariate Analysis of Variance (PERMANOVA; Anderson, 2001; McArdle & Anderson, 2001) based on an Euclidean distance metric was applied to test for statistically significant differences between the groups. Initially, a permutational test (10000 permutations) over all groups was performed at a significance level of $\alpha = 0.05$, followed by three pairwise tests to evaluate which pair of groups was the most similar/different. In the latter, a Bonferroni correction for multiple tests was applied resulting in a significance level $\alpha = 0.0167$.

3.3 ROV observations and coral sample

Two ROV dives (Fig. 2) were conducted using a Sub-Atlantic Cherokee-type ROV “Genesis” guided by a Global Acoustic Positioning System (GAPS) in order to photographically groundtruth the mini-mounds observed on the swath bathymetry. A coral grab sample was collected from which three polyps were selected for U-Th dating. The samples were carefully cleaned in order to avoid contamination from

possible Fe-Mn coatings, detrital sediments and remnants of organic tissue, following the procedures described in Copard et al. (2010). Powdered subsamples were passed through an X-ray diffractometer (XRD) at GEOPS (Geoscience Paris-Sud, Orsay, France) to insure against diagenetic recrystallization of the coral aragonite. Uranium and thorium isotopes were analysed at the Laboratoire des Sciences du Climat et de l'Environnement (LSCE) in Gif-sur-Yvette (France). After adding a triple ^{229}Th ^{233}U-^{236}U spike in a Teflon beaker, the clean samples (ca. 200 mg) were dissolved with diluted HCl. U and Th were coprecipitated with $Fe(OH)_3$, and then separated using UTEVA resin (Eichrom Technologies; Horwitz et al., 1992) in 3N HNO_3. Uranium and thorium isotopes were determined simultaneously using a ThermoScientific NeptunePlus multicollector-ICP-MS fitted with a jet interface. The procedure (chemical separation and analysis) is detailed in Pons-Branchu et al. (2014). After the isotopic data was corrected for peak tailing, hydrate interference and chemical blanks, ages were calculated by iterative age estimation.

3.4 Physical oceanography

Two CTD casts (Fig. 2) were taken down to 1500 m at station B0914-CTD-1 and 450 m at station B0914-CTD-2 using a Seacat SBE-19 deep-water CTD profiler. Temperature, pressure and conductivity were recorded continuously and binned at 1 m resolution and salinity and potential density were derived with the SBE Dataprocessing software (v7.18c). The depth position of the different water masses was determined based on Θ -S mixing triangles between end-members of (1) ENACWst ($\Theta \approx 12.2°$ C, $S \approx 35.66$; Harvey, 1982), (2) ENACWsp ($\Theta \approx 8.56°$ C, $S \approx 35.23$; Castro et al., 1998), (3) MOW at Cape St-Vincent ($\Theta \approx 12.2°$ C, $S \approx 36.6$; Ambar & Howe, 1979) and (4) LSW ($\Theta \approx 3.5°$ C, $S \approx 34.89$; Talley & McCartney, 1982; Cunningham & Haine, 1995). The MOW core was defined as water with > 40% fraction of MOW end member following García Lafuente et al. (2008). This data, collected in May 2009 was combined with World Ocean Database 2013 (WOD13) CTD data collected between 1990 and 1996 before the onset of seasonal upwelling (March to May; Varela et al., 2005; García Lafuente et al., 2008) to construct salinity and temperature profiles at the position of the reflection seismic data using Ocean Data Viewer (Fig. 4).

In order to assess the interactions of M2 internal tides with the Ferrol canyon head topography, a map of the internal tide reflection condition γ/c (Cacchione et al., 2002) was calculated. Here γ is the slope of the topography and c is the angle of the characteristics (also called energy rays or beams) of the internal tides which is determined by:

$$c = \left(\frac{(\sigma^2 - f^2)}{(N^2 - \sigma^2)}\right)^{\frac{1}{2}} \quad (1)$$

where σ is the internal wave-frequency which for M2 internal tides is σ = 0.081 cycles per hour (cph), $f = (\sin\phi/12)$ cph is the local inertial frequency at latitude ϕ and N is the Brunt-Väisälä or buoyancy frequency:

$$N\ (in\ cph) = \frac{3600}{2\pi}\left(\frac{(-g/\rho)}{(\partial\rho/\partial z)}\right)^{\frac{1}{2}} \quad (2)$$

Here, $\partial\rho/\partial z$ is the ocean vertical density gradient and $g \approx 9.81\ \mathrm{m/s^2}$ is the gravitational acceleration. A profile of the buoyancy frequency was derived from the CTD data by first smoothing the temperature and salinity profiles (binning at 10 m intervals and fitting a cubic spline) after which N was calculated using the Gibbs Seawater equation of state routine (TEOS10; IOS et al., 2010; Roquet et al., 2015) implemented in the "oce" R package (Dan & Clark, 2017). From this profile, *c* was calculated according to equation (1) and interpolated on every grid point of the 15 m gridded bathymetry map using ESRI Arcmap 10.1 Spatial Analyst and the arcpy module. Finally, a slope map γ was derived from the bathymetry data and averaged over 2000 m^2 grid areas after which it was divided by the *c* grid to obtain the internal tide reflection condition map.

4. Results

4.1 Geomorphologic analysis

4.1.1 Tectonic features

The acoustic basement of the study area is characterized by a horst structure and a tilted block delimited by normal faults (Fig. 4a) with a WSW-ENE orientation (Fig. 3b; Boillot & Malod, 1988). The seismics reflections of the overlying units are tectonically deformed (Fig. 4). In the western part of the study area, these basement blocks crop out from below the Ortegal Spur marginal platform and form WSW-ENE oriented structural highs at the southern edge of Ferrol Canyon and to the north of the A Coruña Canyon (Fig. 3b). These basement outcrops are characterized by a rugged relief with steep slope angles (up to 40°) and high average backscatter intensity (~ -25 dB; Fig. 3a). In the northern part of the

Ferrol canyon head and in the northern part of the Ortegal Spur marginal platform, similar WSW-ENE oriented structural highs occur in association with normal faults (Fig. 3b). Since no seismic profiles were collected over these features, they were classified as undefined basement outcrops. Several smaller WSW-ENE oriented faults are also present throughout the SE of the Ortegal Spur marginal platform (Fig. 3b) and are associated with a minor offset of the deeper seismic reflections (Fig. 4).

4.1.2 Erosional features

Erosional and abraded surfaces

The walls of the Ferrol and A Coruña canyon heads are formed by several erosional surfaces situated between 450-700 m depth (Fig. 3b). These erosional surfaces have high average backscatter intensity (-20 to -28 dB; Fig. 3a) and their subsurface seismic appearance is characterized by truncated reflections (Fig. 4b, 4c). The erosional surface at the A Coruña canyon head is 0.3-1.5 km wide and forms an escarpment with slope angles of up to ~ 20° (Fig. 3b). In the south, this escarpment has a SW-NE orientation and a height of ~ 20 m which gradually increases towards the SW. After changing direction to a SSW-NNE orientation it reaches a height of up to ~ 100 m (Fig. 4c) and is interrupted by the outcropping basement to the north (Fig. 3b). The erosional surface in the central part of the study area forms a 1.4 km wide E-W oriented escarpment with a slope angle of up to ~ 12° (Fig. 3b) on its southern end. To the north, it curves to a SW-NE orientation, broadens to ~ 5 km while the slope angle decreases to ~ 3° (Fig. 4b) before it eventually disappears below a drift (Fig. 3b). At the most proximal part of the Ferrol canyon head, the erosional surface has a relatively constant width of ~ 1 km and forms an escarpment with slopes angles of ~8°. From south to north it first has a N-S orientation with height of ~ 40 m, then gradually becomes higher up to ~ 60 m as it changes to an E-W orientation (Fig. 3b).

An abraded surface occupies the central part of the Ferrol canyon head, between 550-1000 m depth (Fig. 3b). Compared to the smooth erosive surfaces, it has an irregular relief characterized by furrows that truncate the seafloor-parallel reflections of the deeper strata (Fig. 4b). It is characterized by high average backscatter intensities (-22 dB; Fig. 3a) and a relatively low average slope angle of ~ 3°, although significant local variation in backscatter intensity and slope occur.

Channels

The area hosts several slope-parallel to slope-oblique oriented channels associated with contourite drifts, termed “contourite channels” or “moats”. Most noticeable are the moats that run along the base of the escarpments formed by the erosional surfaces (Fig. 3b). They closely follow the shape of the erosional surface as it changes orientation (Fig. 3b) and are characterized by similar backscatter values (-20 to -28 dB; Fig. 3a). In cross section, the moats have an asymmetric V-shape with the steeper wall facing basinward, truncating the reflections that constitute the Ortegal Spur marginal platform (Fig. 4c). A 12 km long moat up to ~ 700 m wide and ~ 30 m deep occurs near the A Coruña canyon head (Fig. 3b, 4c). In the central part of the study area, a 4 km moat with limited width ~ 100 m and depth ~ 1 m is developed (Fig. 3b). The largest moat of up to ~ 20 km long, ~ 600 m wide and ~ 14 m deep is located at the base of the Ferrol canyon head walls and evolves from an along-slope orientation to a slope-oblique orientation as it follows the erosional surface (Fig. 3b). Several smaller contourite channels with an orientation perpendicular to the overall slope trend run along the base of the WSW-ENE oriented structural highs formed by the outcropping basement or the abraded surface (Fig. 3b) and incise into the basement and the overlying strata (Fig. 4a).

On the Ortegal Spur marginal platform at shallower (450-600 m) water depths, a cross-slope oriented U-shaped channel occurs at the edge of the study area along the base of a SW-NE oriented outcropping basement block (Fig. 3b). This channel is not associated with an apparent contourite drift and was not classified as a contourite channel. The absence of seismic data in this area did not allow further investigation of this feature and hence it was not discussed.

Furrows

The abraded surface and the outcropping basement between 550-1000 m depth are incised by many rectilinear to sinusoidal furrows which are predominantly parallel to the slope, although furrows oblique and even perpendicular to the overall slope also occur (Fig. 3b). The furrows exhibit very high average backscatter intensities (-20 dB) with occasional lower backscatter intensity (-30 dB) patches on their basinward rim (Fig. 3a). In cross section they display V to U shaped incisions that truncate the seismic reflections on their walls (Fig. 4b) They are between 0.4-7 km long, 100-300 m wide and incise the stratigraphy up to ~ 80 m deep (Fig. 3b).

Blind valley

At the SW edge of the Ortegal Spur marginal platform, immediately overlying a large normal fault associated with a basement horst structure, a blind valley is identified (Fig. 3b). The valley has slopes of up to ~ 10° which exhibit a higher backscatter intensity (~ -25 dB) than the surrounding seafloor (~ -30 dB) and the channel axis (~ -30 dB; Fig. 3a). It has a V-shaped cross section which cuts the underlying reflections (Fig. 5c). Near its head, it is about 300 m wide and 4 m deep but widens to 1000 m and deepens to 7 m and near the edge of the sedimentary platform where it ends onto the erosional surface.

4.1.3 Depositional features

Contourite drifts

Contourite drifts, lenticular shaped sediment bodies with an upwardly convex geometry, smooth topography and low average backscatter values (-30 dB; Fig. 3a) occur throughout the study area between 450-1300 m depth(Fig. 3b). They are subdivided into four types: Mounded elongated and separated drifts, confined drifts, mounded patch drifts, and plastered drifts.

Two mounded, elongated and separated drifts exist downslope from the moats at the base of the erosional surfaces (Fig. 3b). In cross section, they are characterized by mounded stratified high amplitude reflections displaying an upslope progradation (Fig. 4c). As the deposit extends basinward, it decreases in thickness (Fig. 4c). The largest such drift is present near the A Coruña canyon head and is ~ 20 km long and ~ 5 km wide. Noticeably, the drift closely follows the changes in the orientation of the topography and continues to the west, outside the study area (Fig. 3b). The eastern edge of the drift has a crest of 8 m above the moat and it gradually becomes higher towards the west with a maximum of 40 m. In the central part of the area, a smaller separated mounded drift is present, elongated along the SW-NE oriented erosional surface (Fig. 3b). It is ~ 6 km long and ~ 5 km wide and has an elevation of about 2 m at the drift crest. It decreases in height towards the NW until it disappears where the erosional surface broadens (Fig. 3b).

In the Ferrol canyon head, two confined drifts are delimited by contourite channels running along the base of the steep erosional surface and the structural highs formed by the outcropping basement (Fig. 3b). They have a mounded morphology which is most defined adjacent to the channels on their western and northern boundary (Fig. 3b). The confined drift located along the N-S oriented erosional surface is ~ 3 km wide and ~ 6 km long and reaches an elevation of 5 m along the channels on its northern and western

edge. The northern most confined drift is ~3 km wide, ~ 8 km long and reaches an elevation of up to ~ 20 m adjacent to the moat at the base of the E-W oriented erosional surface (Fig. 3b).

Two small mounded patch drifts of ~ 1.5 km wide and ~ 2 km long with a crest elevation of ~ 10 m are deposited on the abraded surface and are laterally connected to a larger plastered drift (Fig. 3b). This plastered drift is located at 460-640 m depth on the broad erosional surface and outer Ortegal Spur platform along an EW-oriented contourite channel (Fig. 3b). In cross section it exhibits low mounded, high amplitude reflections that prograde downslope towards the channel (Fig. 4a). The drift is ~ 4 km wide and ~ 7 km long and is elongated in an E-W direction. Its crest has an elevation of ~ 20 m above the moat.

Sediment waves

On the surface of the confined drift in the Ferrol canyon head, a sediment wave field is present at 580-670 m depth (Fig. 3b). The asymmetric waves are oriented perpendicular to the slope with the lee side pointing in the upslope direction. Some of the wave lee sides are characterised by higher average backscatter intensity (-20 dB; Fig. 3a). The waves have a wave height of ~ 1 m, a wavelength of ~ 400 m and narrow, relatively straight crests of 0.6-2 km long.

4.1.4 Mixed (erosional and depositional) features

The most noticeable feature of the study area is the large contourite terrace which forms the upper slope part of the Ortegal Spur marginal platform between 200-600 m depth (Fig. 3b). Its landward boundary is not defined as it lies outside the study area but likely coincides with the shelf break at ~ 200 m depth. Its basinward boundary is formed by the steep erosional surfaces. To the south of the Ferrol canyon head, this terrace reaches a width of up to 20 km and dips toward the NW while to the north of the Ferrol Canyon it dips towards the SW (Fig. 3b). The upper part of the terrace reaches down to 500 m depth, has a slope angle of 0-2° and is characterized by a high average backscatter intensity (-38 dB; Fig. 3). Its subsurface seismofacies consists of high amplitude seafloor-parallel to chaotic reflections which fill in the topography of the tectonically deformed strata below (Fig. 4, 5a, 5b), indicating a dominant depositional regime. In contrast, the outer part of the terrace has a steeper slope angle of 2-4° and a higher average backscatter intensity of -28 dB (Fig. 3a). It has a variable width of 1-5 km and its seismofacies is characterized by truncated reflections (Fig. 4, 5c) indicating a dominant erosional regime. In the central part of the study area, the erosional surface broadens and the lower boundary of the terrace is not well defined. Here, the outer part of the terrace is covered by a plastered drift (Fig. 3b, 4a).

4.1.5 Mass wasting features

Mass wasting deposits are uncommon in the study area with the exception of a slide scar and slump deposit at the edge of the A Coruña Canyon axis which occurs just to the south of the study area (Fig. 3b). The slide scar is ~ 7 km long and up to ~ 30 m high and has a complex shape with several amphitheatre shaped subsections (Fig. 3b).

4.1.6 Fluid migration features

In the eastern and south-eastern part of the study area between 250-450 m depth, 55 pockmarks, circular to oval seafloor depressions occur (Fig. 3b). They are part of a larger pockmark field on the Ortegal Spur, which extends towards the east outside the study area (Jané et al., 2010). Their morphological characteristics (Table 1) fall within standard pockmark dimensions (Pilcher & Argent, 2007) and are in agreement with those derived for the entire Ortegal Spur pockmark field (Jané et al., 2010). These features have low average backscatter intensities (-37 dB) although some exhibit higher intensity (-30 dB) patches on their rim and slopes (Fig. 3a).

On the seismic profiles, the pockmark are characterised by seafloor depressions which truncate the uppermost reflections and in some cases, an elevated rim is observed (Fig. 5a, 5b). Several acoustic anomalies related to fluid migration occur in the underlying strata (Fig. 5a, 5b): vertical dim and wipe out zones, bright spots, dim spots and intra-sedimentary doming (Hovland & Judd, 1988; Løseth et al., 2009).

4.1.7 Biogenic features

On the Ortegal Spur, 171 small circular mounded features occur both to the north of Ferrol canyon head ("northern mini-mounds") as well as to the south-east of the canyon head ("southern mini-mounds"), adjacent to the pockmark field. They are present between 400-550 m depth on both the depositional and erosional part of the contourite terrace (Fig. 3b). The mini-mounds on both side of the canyon have different morphological characteristics (Table 1). The southern mini-mounds have a larger diameter and a more dispersed distribution while the more numerous northern mini-mounds are smaller and more clustered. Mound height and slopes are relatively similar with slightly higher values for the southern mini-mounds (Table 1). The mounds display average backscatter values of -27 dB and they thus turn up as brighter dots on the low backscatter (-38 dB) depositional region of the terrace (Fig. 3a, 6). On the erosional, outer part of the terrace with higher average backscatter intensity (-28 dB), the mounds display

a high backscatter centre (-27 dB) with a low backscatter rim (-35 dB; Fig. 3a). Some circular high backscatter patches, not associated with seafloor elevations, are apparent however they were not interpreted as mini-mounds.

On the seismic profiles, the southern mini-mounds exhibit small elevations of the seafloor reflection without any subsurface expression (Fig. 5c, right mound). However, in some of the mounds, the underlying strata display several acoustic anomalies related to fluid flow (Løseth et al., 2009): vertical dim zones, discontinuities and dim spots (Fig. 5c, left mound). Pull-up of the reflections below the mound indicates a local increase of sound velocity within the mini-mound. No seismic profiles were acquired over the northern mini-mounds.

The seafloor facies of the mini-mounds was characterized by bioturbated mixed bioclastic and siliciclastic sand with scattered coral rubble (Fig. 6a, 6c). The coral rubble consisted predominantly of fossil *L. pertusa* branches as well as large, mostly buried coral framework (Fig. 6a). Although the off-mound areas were not extensively explored, the area between and at the edge of the mounds was devoid of coral rubble, consisting only of mixed bioclastic and siliciclastic sands (Fig. 7b, 7c). Sedimentary bed forms related to bottom currents were not observed. Although the fossil *L. pertusa* rubble was abundant, no living scleractinians were observed. U-Th dating of a large coral sample revealed it developed between 9.64-9.34 ± 0.03 ka BP (Table 2). Low ^{232}Th concentrations (< 0.4 ppb; Table 2), within the range of well-cleaned modern corals (0.1-2.4 ppb; van de Flierdt et al., 2010) indicate that the cleaning method was successful in removing contaminants. Furthermore, $\delta^{234}U_o$ values are within the 5 ‰ range criterion (Dutton & Lambeck, 2012) of modern sea water (146.8 ± 0.1 ‰; Andersen et al., 2010) used as a reference for the detection of closed system behaviour of the coral and hence these ages are considered to be reliable (Table 2).

4.2 Morphometric analysis of mini-mounds and pockmarks

The principal component analysis indicates that the morphological characteristics of the southern mini-mounds and the pockmarks form largely overlapping clusters (Fig. 7), indicating similarity in the feature morphology. However, the pockmarks seem to have a slightly more elongated shape (smaller width to length ratio) and a smaller azimuth of the elongated axis. The characteristics of the northern mounds, even though largely overlapping with the other features, are clearly different (Fig. 7). This

difference is captured by the first principal component that loads primarily on the nearest neighbour distance and mean feature diameter, indicating that the northern mounds are both smaller in size and more clustered compared to the other groups (Fig. 7). The PERMANOVA test over all groups indicates a highly significant difference in morphological characteristics between at least one pair of the feature groups (Table 3). Follow-up pairwise tests indicate that, considering a Bonferroni correction of the significance level $\alpha = 0.0167$, the morphological characteristics of the pockmarks and southern mini-mounds are not significantly different (Table 3). In contrast, a highly significant difference results from the comparison of both pockmarks with northern mini-mounds and northern with southern mini-mounds (Table 3).

4.3 Oceanography

4.3.1 Water masses and their interfaces

The collected CTD data is displayed in Fig. 8. The seasonal thermocline was observed around 75 m depth. At the shallow station (CTD2 in Fig. 2, dashed line in Fig. 8) between 75-400 m, the temperature and salinity decreased from 12.5° C to 11.4° C and 35.75 to 35.65 respectively. Below, the salinity increased to 35.7 at bottom of the station (450 m depth) while temperature remained constant. At the deep station (CTD 1 in Fig. 1, full line in Fig. 8), the water column between 75-500 m depth was characterized by similar salinity (35.6-35.7) and temperature (11-12° C.) values. A salinity minimum was observed at 500 m depth, below which salinity increased reaching a maximum of 36.1 at 900 m (Fig. 8a). The temperature reached a local minimum of 10.6° C around 650 m depth below which it increased to a local maximum of 11.4° C at 800 m. Between 800-1150 m depth, temperature and salinity remained within a narrow T-S envelope (10.5-11.5° C and 36.0-36.1). Below, both temperature and salinity decreased to 7.6° C and 35.6 respectively at the bottom of the station (1500 m ; Fig. 8a).

Θ -S mixing triangle calculations (Fig. 8b) indicate that ENACW occupied the water column between 75-600 m depth at the deep site (CTD1) and was the only water mass observed at the shallow site (CTD2). The MOW core was observed between 740-1470 m depth (dark grey zone in Fig. 8). The depth interval 600-740 m corresponded to a mixing zone between the ENACW and the MOW where the contribution of MOW changed from 20% to 40% (light grey zone in Fig. 8). Although LSW was not observed in the study area, its influence increased from 0.5 % to 45 % between 1150-1500 m depth where it mixed with the

lower MOW boundary. The pycnocline and hence the maximum in buoyancy frequency occurred between 500-900 m depth and corresponds to the lower ENACW, the ENACW-MOW mixing zone and the upper MOW core (Fig. 8c). These results were collected in May before seasonal upwelling sets in and are generally consistent with the March to May WOD13 data (Fig. 4) and results from García Lafuente et al. (2008).

4.3.2 Internal tide topography interaction

The ratio of the slope of the topography γ to the angle of the characteristics of M2 internal tides c (equation 1) determines how the characteristics will be reflected upon interaction with the continental margin topography (Cacchione & Wunsch, 1974; Cacchione et al., 2002). Where the slopes are subcritical ($\gamma/c < 1$) or supercritical ($\gamma/c > 1$) the incoming internal tides will be reflected upslope ("transmissive") or reflected downslope ("reflective") respectively about the direction of the local gravity vector. However, when the slopes are at a critical angle ($\gamma/c \approx 1$), the wave energy becomes trapped along the bottom layer resulting in breaking of the waves and increased bottom current velocities and bottom shear stress (Cacchione et al., 2002; Lamb, 2014). Critical slopes are also areas of internal tide generation, where they interact with the barotropic tide (Balmforth et al., 2002; Zhang et al., 2008), a process which also results in enhanced bottom current velocities (Lamb, 2014). Such critical conditions for M2 internal tides are present within the Ferrol canyon head, at the location of the abraded surface, the sediment wave field and the contourite drifts (Fig. 8d). The steep slopes of the erosional surfaces at the canyon head walls and the outcropping basement ridges are supercritical (Fig. 8d). Interestingly, on the contourite terrace at the Ortegal Spur, the outer erosional region is characterized by near-critical conditions, while the depositional part of the terrace is sub-critical (Fig. 8d). It should be noted that the density profile changes during seasonal upwelling and downwelling events (García Lafuente et al., 2008) hence the N profile and critical reflection map may also display seasonal changes (Cacchione et al., 2002) which were not evaluated.

5. Discussion

5.1 Sedimentary and Oceanographic processes

Detailed geomorphological analysis of the Ferrol canyon head and Ortegal Spur reveals a complex interplay of tectonic processes which control the large scale morphology (Maestro et al., 2013) through

the uplift of large WSW-ENE oriented structural highs delimiting the submarine canyons (Fig. 3b, 4a) and sedimentary processes controlling the wide variety of identified seabed morphologies at a more local scale (Fig. 3b). Many of the observed erosional (erosional and abraded surfaces, contourite channels and furrows), depositional (contourite drifts and sediment waves) and mixed features (contourite terrace) demonstrate a dominant control of bottom currents on the sedimentary processes (Rebesco et al., 2014). This was first recognised by Hernández-Molina et al. (2011) who described the sedimentary architecture of the Ortegal Spur as a contourite depositional system (CDS) connected to the MOW. The MOW acts as a northward density driven slope current with a speed proportional to the density difference with the surrounding water masses and the slope of the topography (Price & Baringer, 1994; Baringer & Price, 1999; Iorga & Lozier, 1999b; Legg et al., 2009; Hernández-Molina et al., 2011). The change in regional slope trend at the Ortegal Spur forms an obstacle to this boundary current as it flows around the Ortegal Spur and into the Bay of Biscay (Iorga & Lozier, 1999b; García Lafuente et al., 2008), locally enhancing its velocity (Hernández-Molina et al., 2011).

The CTD data, collected before the onset of seasonal upwelling, indicates that the contemporary MOW reaches up to 740 m depth while the mixing zone with the overlying ENACW reaches up to 600 m (Fig. 4, 8). However, during the upwelling season, the MOW core and mixing zone are displaced upslope by as much as 100 m (García Lafuente et al., 2008; Prieto et al., 2013). The identified erosional and depositional features in the Ferrol Canyon and A Coruña canyon heads (Fig. 3b) are thus, either continuously or seasonally, influenced by this water mass. It's impact on the sedimentary regime in the Ferrol canyon head is indicated by the moats and mounded contourite drifts at the base of the steep erosional surfaces which form the canyon walls and against outcropping basement ridges (Faugères et al., 1999; Rebesco et al., 2014). Here, the MOW density current is focused against the steep topography by the coriolis force (McCave, 1982), resulting locally in high bottom current velocities and erosion within the moats and along the steep wall (Fig. 4c). Due to bottom friction, a secondary flow (Ekman transport) develops within the bottom boundary layer of the current core which is oriented downslope, oblique to the main flow (Wåhlin & Walin, 2001; Rebesco et al., 2014). As a result, the eroded sediment is transported downslope, where bottom current velocities are lower and deposition results in the formation of mounded contourite drifts adjacent to the moats (Fig. 4c; Faugères et al., 1999; Llave et al., 2007). On the southern flank of the WSW-ENE basement ridges and E-W oriented erosional surface, this along-slope flow is steered in a downslope

direction as evidenced by moats and drifts crossing the isobaths along the base of these features (Fig. 3b). This downslope steering of along-slope density driven currents by topographic obstacles has been described from modelling and observation (Darelius & Wåhlin, 2007) and was recreated in laboratory experiments (Darelius, 2008). In the central part of the study area, the broad erosional and abraded surfaces (Fig. 3b) have a lower average slope angle and likely indicate the presence of less confined tabular bottom currents (Rebesco et al., 2014). Local variation in the bottom current velocities due to interaction with the irregular topography of the abraded surface and outcropping basement likely resulted in the incision of furrows with steep basinward facing walls parallel to oblique to the isobaths (Fig. 3b, 4b; Stow et al., 2002; Rebesco & Camerlenghi, 2008; Hernández-Molina et al., 2011; Rebesco et al., 2014).

The conceptual model of topographic steering of the MOW density current explains many of the along-slope oriented features as well as slope-oblique oriented features near topographic obstacles. However, the sediment wave field with crests parallel to the isobaths as well as several slope-perpendicular furrows cannot be explained by along-slope processes and suggest a more cross-slope oriented process associated to the bottom currents (Fig. 3b). The sediment waves' sinuous crest shape and dimensions are characteristic for sand waves which generally have wavelengths of 5-500 m and wave heights of 0.5-5 m (Stow et al., 2009). Their asymmetry suggest an upslope migration (Wynn & Masson, 2008). The assumption of sandy sediment based on the wave morphology is supported by the observation of fine to medium sand on the upper NW Iberian slope (Flach et al., 2002; van Weering et al., 2002). Such sand waves generally form under the influence of bottom currents perpendicular to the wave crests with velocities between 0.30-0.75 m/s (Stow et al., 2009). Furthermore, furrows crossing the isobaths on the abraded surface suggest cross-slope bottom current velocities > 0.30 m/s in the case of muddy sediment or > 0.60 m/s in case of sandy sediment (Stow et al., 2009). These features are situated on a slope critical to M2 internal tides (Fig. 8d) and hence an important component of the cross-slope bottom currents is likely generated by breaking of internal tides and formation of tidal bores upon interaction with the critical slopes (Cacchione et al., 2002; Lamb, 2014). Cross-slope oriented, baroclinic bottom currents up to 0.19 m/s at M2 frequency have been reported on the open slope at 1100 m depth to the south of the study area (García-Lafuente et al., 2006). Within the Ferrol canyon head, such baroclinic currents are expected to be intensified for two reasons: (1) The position at pycnocline depth, where stratification (and hence

buoyancy frequency) is at a maximum (Fig. 8c), results in an efficient conversion of barotropic to baroclinic tide energy over the critical slopes (Baines, 1982; Zhang et al., 2008; Vlasenko et al., 2014); (2) focussing of internal tides by downward reflection of incoming internal tide beams at the supercritical erosional surfaces of the canyon head walls (Fig. 8d) concentrates the tidal energy along the critical bottom layer in the canyon head below (García-Lafuente et al., 2006; Vlasenko et al., 2016). This interaction of tidal currents (both barotropic and baroclinic) with canyon topography has been reported to generate bottom currents with velocities that commonly range between 0.25-0.50 m/s (Shepard, 1975; Shanmugam, 2003; Pomar et al., 2012) although several authors have reported maximum velocities of up to 1 m/s (Lee et al., 2009; Mulder et al., 2012). This process thus generates bottom currents of sufficient magnitude to form the observer furrows and sediment waves in the Ferrol canyon head. Internal tide and wave activity has also been proposed as a formation mechanism for sediment waves near pycnoclines in the Bay of Biscay (Faugères et al., 2002; Delivet et al., 2016) and on other continental slopes (He et al., 2008; Reeder et al., 2011; Preu et al., 2013; Belde et al., 2015; Ribó et al., 2016; Hernández-Molina et al., 2017).

Contourite terraces, like the one on the Ortegal spur (Fig. 3b, 4), are typically associated with water mass boundaries and their low mounded shape is the result of erosion through the persistent action of internal waves and tides associated with the pycnocline at these boundaries (Hernández-Molina et al., 2009; Preu et al., 2013; Hernández-Molina et al., 2016; 2017). The Ortegal spur contourite terrace is situated at 200-600 m depth (Fig. 3b) above the contemporary ENACW-MOW interface (Fig. 8c). This suggests that the interface was in a shallower position in the past. In the present day, resuspension and erosion by bottom currents is restricted to the outer part of the terrace below 450 m depth (Fig. 3b, 4) which coincides with the upper edge of the pycnocline (Fig. 8c). The slope of this region is near-critical to M2 internal tides (Fig. 8d) and hence the erosional regime on the outer terrace may also be attributed to generation and breaking of internal tides (Lamb, 2014). The plastered drift at the base of the terrace (Fig. 3b, 4c) is likely formed by an unconfined along-slope current over the broad erosional surface which transports the resuspended sediment and deposits it against the outcropping basement ridge to the north. In contrast, the depositional part of the terrace (Fig. 3b, 4) lies outside the present-day pycnocline (Fig. 8c) and slopes are subcritical (Fig. 8d). Here bottom currents are insufficient to resuspend the observed mixed biogenic siliciclastic sands (Fig. 6b) resulting in a depositional regime.

The dominance of erosional features around the Ferrol canyon head indicates that the area is subject to active sediment resuspension. The resuspended sediment likely contributes significantly to the formation of the intermediate nepheloid layer reported at 500-800 m depth along the NW Iberian margin (McCave & Hall, 2002). In addition to sediment resuspended from the shelf-edge (McCave & Hall, 2002; van Weering et al., 2002), the Ferrol canyon head might act as an important source area for sediment transported to the deeper ocean. If this is the case, it likely also contributes sediments to the large plastered drift of the Ortegal CDS located downslope (Llave et al., 2015).

5.2 mini-mounds

5.2.1 Early stage CWC mounds

The observed association of fossil *L. pertusa* rubble with the mini-mounds (Fig. 7a, 7c) suggests that these seafloor elevations are biogenic structures formed by CWC growth. This cover of fossil CWC rubble explains the higher backscatter intensities observed on top of many of the mounds (Fig. 3a, 6d). CWC reefs are thought to initiate by settling of coral larvae on firm and preferentially elevated substrate (Wheeler et al., 2007; de Haas et al., 2009). As the reef grows, the older polyps at the bottom of the coral framework die and the exposed skeleton becomes susceptible to bio erosion (Beuck & Freiwald, 2005). The resulting coral rubble falls down and extends the perimeter of the reef patch, providing settle ground for new generations of larvae (Roberts et al., 2006). The coral framework slows down the bottom currents by frictional drag and thus baffles bypassing sediment. This locally enhances sedimentation rates and results in the formation of a mounded biogenic structure (Dorschel et al., 2005; de Haas et al., 2009; Mienis et al., 2009; Eisele et al., 2014). If favourable conditions for coral growth are present or recurrent over long time scales, individual reefs are able to coalesce and form giant mounds (e.g. Belgica Mound Province; De Mol et al., 2005) which have a "developed morphology" shaped by the prevailing hydrodynamic conditions (Wheeler et al., 2007). However, in the early stages of this process, the mound will have a more or less "inherited morphology", which resembles that of the initially colonized substrate (Wheeler et al., 2007). The mini-mounds near the Ferrol canyon head, with their limited elevation (1.9-2.7 m) and lack of subsurface expression (Fig. 5c), likely resulted from a short-lived episode of mound development and hence belong to the latter category.

Contemporary analogues for such early stage CWC mini-mounds were reported in the Porcupine Seabight (Moira Mounds; Foubert et al., 2011; Wheeler et al., 2011), in the Rockall Through (Darwin Mounds; Huvenne et al., 2009a; Victorero et al., 2016) and on the Galicia Bank (Somoza et al., 2014). In contrast to these mounds, which support a living CWC framework, no living coral was observed on the explored Ferrol Canyon mini-mounds (Fig. 6c). The cessation of CWC growth, likely resulting from a change to unfavourable environmental conditions (see section 5.2.3), led to the collapse of the reef framework after which it becomes filled in with sediment. Erosion by bottom currents or organisms living on top of the extinct mound then resulted in the observed seafloor facies of mostly buried *L. pertusa* framework and rubble on the mini-mounds (Fig. 6a; Dorschel et al., 2005; Douarin et al., 2014). Such relict CWC mini-mounds with comparable dimensions (50-250 m in diameter, < 10 m high) have been reported at similar water depths (250-550 m) near the head of submarine canyons in the Bay of Biscay: Celtic margin (Stewart et al., 2014); Armorican margin (De Mol et al., 2011) and Cantabrian margin (Sánchez et al., 2014).

5.2.2 Role of seepage

The close proximity of the pockmark field upslope from the southern mini-mounds triggers the question whether there is a genetic link between these features. The Ortegal Spur pockmarks are thought to be created by seepage of thermogenic gas and/or other pore fluids from Late Cretaceous units migrating upwards along basement faults (Jané et al., 2010) which also underlie the mini-mounds (Fig. 3b). The observation of seismic anomalies (Løseth et al., 2009) suggests vertical and lateral fluid migration below both the pockmarks and some of the mounds (Fig. 5), indicating a potential role of seepage processes in mini-mound formation.

Mound morphology and spatial distribution, expected to be inherited from the colonized feature (Wheeler et al., 2007), is not significantly different between the southern mini-mounds and the adjacent pockmarks (Table 3; Fig. 7). Pre-existing pockmarks may thus have provided preferential colonization surfaces for CWC larvae. Authigenic carbonate cementation of soft sediments, often found in pockmarks and other seepage sites (Friedman et al., 1988; Hovland & Judd, 1988; Boetius et al., 2000; Greinert et al., 2001; Magalhães et al., 2012) could have provided hard grounds, required for the attachment of coral polyps and the initiation of reef growth (Wheeler et al., 2007; de Haas et al., 2009). Although no direct seafloor observation of authigenic carbonate slabs in the Ortegal Spur pockmarks have been made, their

presence could explain the observed patches of higher backscatter intensities on the slopes and rim of these features. This process, where seepage features influence CWC mound initiation, has been proposed for several CWC mound provinces (Kellogg et al., 2009; Wehrmann et al., 2011; Magalhães et al., 2012; Somoza et al., 2014).

In contrast, the smaller and more clustered northern mini-mounds have a significantly different morphology from both the southern mini-mounds and the pockmarks (Table 3; Fig. 7). These mounds have a similar degree of clustering as observed for mini-mounds on the Celtic (Stewart et al., 2014) and Armorican margin (De Mol et al., 2011) where pockmarks have not been identified. In the absence of pre-existing pockmarks, these mounds may have initiated by larvae colonization on smaller firm features like dropstones (Wheeler et al., 2007; Victorero et al., 2016). This process however is not exclusive to the northern region and may be responsible for some of the smaller southern mini-mounds or mounds not associated with fluid migration (right mound in Fig. 5c).

5.2.3 Role of oceanographic conditions and anthropogenic impact

The coral mini-mounds are situated within the ENACW water mass at temperatures of 10.8-11.4° C and salinity of 35.6-35.7 (Fig. 8a). This falls within the wide range of temperature (4-14° C) and salinity (32-38.9) reported for living cold-water corals in the NE Atlantic (Rogers, 1999; Freiwald et al., 2004; 2009). The depth range of the mini-mound province overlaps with the upper edge of the pycnocline (Fig. 8c) at 500 m depth which marks the transition between the erosional and depositional region of the contourite terrace (Fig. 3b). The lower part of the coral mound province (below 500 m depth) is thus situated on the erosional region where bottom currents are sufficient to cause resuspension (Fig. 3b). A vigorous bottom current regime like the one observed within the Ferrol canyon head, is important to sustain CWC reefs (White & Dorschel, 2010; Mohn et al., 2014; van Haren et al., 2014) as it significantly enhances the encounter rate of food particles and prevents the corals from being smothered by sediment (White et al., 2005; Dorschel et al., 2007; Davies & Guinotte, 2011; Mienis et al., 2012a; 2012b). Nepheloid layers generated by the bottom currents in this depth interval of the NW Iberian margin have been reported by McCave and Hall (2002). Concentration of organic material within these turbulent layers has been linked to coral occurrence (e.g. Mienis et al., 2007). In contrast, the upper part of the coral mound province (above 500 m depth) is located on the depositional part of the contourite terrace where bottom current velocities are lower and deposition dominates. Conditions in the upper region of the minimound

province are thus unfavourable for coral growth, which is supported by the lack of living *L. pertusa* observed on the mounds in this area (Fig. 6a). If bottom currents were the only limiting factor on coral growth, mound development may still be an on-going process on the lower region which was not explored. However, other factors like low primary production, lack of active larval supply and/or anthropogenic impact may also prevent contemporary coral growth on the mini-mounds. Present day primary production along the Iberian margin is generally high due to the upwelling regime (Bernárdez et al., 2008; Salgueiro et al., 2008) and unlikely to be a limiting factor. In contrast, the potential density envelope σ_θ =27.35-27.65 kg/m^3, suggested to control larvae transport along the NE Atlantic margin (Dullo et al., 2008; Flögel et al., 2014; Rüggeberg et al., 2016), is located outside the mini-mound province at the interface between the ENACW and MOW water mass (600-950 m depth; Fig. 8c). The observation of a living specimen of *Madrepora oculata* in the Ferrol canyon head at 750 m depth (Fig. 4b in Hernández-Molina et al., 2010) indicates that conditions in this depth interval are indeed able to sustain CWC growth. Hence, the fossil mini-mounds are potentially cut off from larval supply inhibiting recolonization of the structures. In addition, the lack of contemporary coral growth might also be related to habitat destruction by bottom trawling (Roberts et al., 2006) as the NW Iberian shelf and upper slope have been subject to extensive fishing activities for several decades (Oberle et al., 2016). Influence of bottom trawling on similar mini-mounds on the Celtic margin has been confirmed by the frequent seafloor observation of trawl marks (Stewart & Davies, 2007) which potentially explains the highly fragmented and exposed *L. pertusa* rubble accumulations observed on these mounds (Stewart et al., 2014). In comparison, no trawl marks were encountered on the Ortegal Spur mini-mound province and the observation of large, buried *L. pertusa* framework (Fig. 6a) suggests a relatively undisturbed seafloor. However, based on the limited explored area (Fig. 6c), the potential impact of trawl fishing and its role in the absence of active CWC growth cannot be ruled out.

5.2.4 Timing and palaeoceanographic implications

The abundance of CWC mini-mounds at 400-550 m water depth indicates that during mound development this area hosted optimal conditions for coral growth. This implies that the pycnocline and the potential density envelope associated with the ENACW-MOW interface was up to 100-200 m shallower than today. When the density profile changed towards its contemporary configuration, CWC likely migrated to more favourable conditions within the Ferrol canyon head, causing the mini-mounds to

become relict features. Alternatively, the introduction of bottom trawling on the upper NW Iberian slope might also have forced this migration as the rough topography in the canyon head provides shelter from trawling activities. A CWC migration into submarine canyons was also reported on the Celtic (Stewart et al., 2014), Armorican (De Mol et al., 2011) and Cantabrian margin (Sánchez et al., 2014). The small dimensions and lack of subsurface expression of the mound structures indicates that they likely developed as a result of a short-lived episode of coral growth during the Holocene. U-Th dating of a single *L. pertusa* branch (9.64-9.34 ± 0.03 ka BP) indicates mound growth was active during the early Holocene. Interestingly, similar ages (9.1-7.4 ka BP) have been reported for the fossil mini-mounds at 250-360 m depth on the Armorican margin (De Mol et al., 2011). Although these preliminary ages suggest a natural cause for the CWC migration, there is a need for a better age constraint on the CWC mini-mound development to rule out an anthropogenic impact.

Considering the available data, we propose the hypothesis that the development of CWC mini-mounds in shallow areas, reported here and on other sites along the Bay of Biscay margin was a regional phenomenon as a result of a shallower ENACW-MOW water mass interface during the early Holocene. The settling depth of the MOW and hence the ENACW-MOW interface has been subject to large changes in the past (Schönfeld & Zahn, 2000; Rogerson et al., 2011; 2012) and is mainly controlled by NE Atlantic density profile changes connected to the Atlantic Meridional Overturning Circulation (AMOC; Rogerson et al., 2011; 2012). The early Holocene is characterized by an overall increased AMOC intensity compared to the LGM and late Holocene as evidenced by several records of Nordic sea overflow (Kissel et al., 2013; Thornalley et al., 2013) and North Atlantic Deep Water export (McManus et al., 2004; Lippold et al., 2016). This is expected to have increased the vertical density gradient within the North Atlantic over several millennia (Rogerson et al., 2011), resulting in a decreased settling depth of the ENACW-MOW interface during time of mini-mound development. The present day water mass configuration on the Iberian margin was established between 7.5 and 5.5 ka when the MOW core retreated to 800 m (Schönfeld & Zahn, 2000) which shifted the favourable conditions for CWC growth to deeper water depth.

6. Conclusions

This study has described the geomorphological features and oceanographic conditions of the Ferrol canyon head and the Ortegal Spur on the NW Iberian upper slope. The identified erosional (erosive and

abraded surfaces, contourite channels and furrows), depositional (contourite drifts and sediment waves) and mixed (contourite terrace) features indicate that sedimentary processes near the canyon head are predominantly controlled by bottom currents. These currents result from the topographic steering of the density driven MOW slope current and from interaction between the canyon head topography and M2 internal tides associated with the pycnocline at the ENACW-MOW interface. Active resuspension within the Ferrol canyon head likely contributes to INL formation and sediment transport to the deeper ocean.

Furthermore, this study has characterized a new province of CWC mini-mounds on a contourite terrace at the edge of the Ferrol canyon head. A novel morphometric approach based on semi-automated mapping and multivariate statistics was applied in order to generate further insights in the relation between the CWC mini-mounds and the Ortegal Spur pockmarks and explain the observed differences in the spatial distribution and morphology. The relict mini-mounds occur upslope from the contemporary ENACW-MOW interface, situated within the canyon head, where enhanced bottom currents and potential density favour CWC growth. Although the position outside of these favourable conditions potentially explains the absence of contemporary coral growth on the mini-mounds, the impact of bottom trawling cannot be ruled out. A preliminary age constraint (9.64-9.34 ± 0.03 ka BP) reveals coral growth occurred during the early Holocene, coeval to relict CWC mini-mounds in a similar setting on the Armorican margin. The existence of these CWC mini-mounds suggests a regional shift in the NE Atlantic density profile, resulting in an early Holocene ENACW-MOW interface which was up to 200 m shallower than in the present. This is potentially connected to an increased AMOC intensity during the early Holocene. As CWC mounds are great paleoclimate archives, further investigation of these mini-mounds could provide key insights in MOW paleoceanography and its influence along the NE Atlantic margin. Furthermore, additional coral dating will allow to distinguish between a natural or an anthropogenic cause for the CWC demise in this setting.

This contribution highlights the important role of bottom current processes on the sedimentary environment in and around canyon heads located on the upper slope and adds to a growing body of research which aims to better understand these processes and their relation to different oceanographic phenomena.

7. Acknowledgements

This study has been funded through the Research Foundation Flanders (FWO) project n° 3G042713 "Mini-mound". U/Th analyses were co-funded by the ANR HAMOC project. The research was conducted in the framework of "The Drifters Research Group" of the Royal Holloway University of London (UK) and it is related to the projects CTM 2012-39599-C03, CGL2016-80445-R and CTM2016-75129-C3-1-R. The authors wish to acknowledge the captain, crew and scientific participants of R/V Belgica Cruise 09/14. Ship time onboard the R/V Belgica was provided by BELSPO and RBINS-OD Nature. The authors also wish to express gratitude to the reviewers for their constructive feedback and to Dr. Thomas Vandorpe, Dr. Stanislas Delivet and Dr. Agostina Vertino for their input and discussion.

8. Bibliography

Allen, S.E., Durrieu de Madron, X., 2009. A review of the role of submarine canyons in deep-ocean exchange with the shelf. *Ocean Sci.*, 5(4), 607-620.

Ambar, I., Howe, M.R., 1979. Observations of the mediterranean outflow—II the deep circulation in the vicinity of the gulf of cadiz. *Deep Sea Research Part A. Oceanographic Research Papers*, 26(5), 555-568.

Andersen, M.B., Stirling, C.H., Zimmermann, B., Halliday, A.N., 2010. Precise determination of the open ocean 234U/238U composition. *Geochemistry, Geophysics, Geosystems*, 11(12), 1525-2027.

Anderson, M.J., 2001. A new method for non-parametric multivariate analysis of variance. *Austral ecology*, 26(1), 32-46.

Arzola, R.G., Wynn, R.B., Lastras, G., Masson, D.G., Weaver, P.P.E., 2008. Sedimentary features and processes in the Nazaré and Setúbal submarine canyons, west Iberian margin. *Marine Geology*, 250(1), 64-88.

Azevedo, A., da Silva, J.C.B., New, A.L., 2006. On the generation and propagation of internal solitary waves in the southern Bay of Biscay. *Deep Sea Research Part I: Oceanographic Research Papers*, 53(6), 927-941.

Baines, P.G., 1982. On internal tide generation models. *Deep Sea Research Part A. Oceanographic Research Papers*, 29(3), 307-338.

Balmforth, N., Ierley, G., Young, W., 2002. Tidal conversion by subcritical topography. *Journal of Physical Oceanography*, 32(10), 2900-2914.

Baringer, M.O., Price, J.F., 1999. A review of the physical oceanography of the Mediterranean outflow. *Marine Geology*, 155(1-2), 63-82.

Belde, J., Back, S., Reuning, L., Eberli, G., 2015. Three-dimensional seismic analysis of sediment waves and related geomorphological features on a carbonate shelf exposed to large amplitude internal waves, Browse Basin region, Australia. *Sedimentology*, 62(1), 87-109.

Bernárdez, P., González-Álvarez, R., Francés, G., Prego, R., Bárcena, M.A., Romero, O.E., 2008. Palaeoproductivity changes and upwelling variability in the Galicia Mud Patch during the last 5000 years: geochemical and microfloral evidence. *The Holocene*, 18(8), 1207-1218.

Beuck, L., Freiwald, A., 2005. Bioerosion patterns in a deep-water Lophelia pertusa (Scleractinia) thicket (Propeller Mound, northern Porcupine Seabight). In A. Freiwald, J.M. Roberts (Eds.), *Cold-Water Corals and Ecosystems* (pp. 915-936). Berlin, Heidelberg: Springer Berlin Heidelberg.

Boetius, A., Ravenschlag, K., Schubert, C.J., Rickert, D., Widdel, F., Gieseke, A., Amann, R., Jørgensen, B.B., Witte, U., Pfannkuche, O., 2000. A marine microbial consortium apparently mediating anaerobic oxidation of methane. *Nature*, 407(6804), 623-626.

Boillot, G., Dupeuble, P.A., Malod, J., 1979. Subduction and Tectonics on the Continental-Margin Off Northern Spain. *Marine Geology*, 32(1-2), 53-70.

Boillot, G., Malod, J.-A., Dupeuble, P.A., CYBERE Group, 1987. Mesozoic evolution of Ortegal Spur, North Galicia margin: Comparison with adjacent margins. In G. Boillot, E.L. Winterer, A.W. Meyer (Eds.), *Proc. Init. Repts ODP*, Vol. 103 (pp. 107-119): Texas A&M University.

Boillot, G., Malod, J.A., 1988. The north and northwest spanish continental margin: a review. *Revista de Sociedad Geologica de Espana*(1), 295-316.

Bourillet, J.F., Zaragosi, S., Mulder, T., 2006. The French Atlantic margin and deep-sea submarine systems. *Geo-Marine Letters*, 26(6), 311-315.

Cacchione, D., Wunsch, C., 1974. Experimental study of internal waves over a slope. *Journal of Fluid Mechanics*, 66(02), 223-239.

Cacchione, D.A., Pratson, L.F., Ogston, A.S., 2002. The Shaping of Continental Slopes by Internal Tides. *Science*, 296(5568), 724-727.

Castro, C.G., Pérez, F.F., Holley, S.E., Ríos, A.F., 1998. Chemical characterisation and modelling of water masses in the Northeast Atlantic. *Progress In Oceanography*, 41(3), 249-279.

Copard, K., Colin, C., Douville, E., Freiwald, A., Gudmundsson, G., De Mol, B., Frank, N., 2010. Nd isotopes in deep-sea corals in the North-eastern Atlantic. *Quaternary Science Reviews*, 29(19-20), 2499-2508.

Cunningham, S.A., Haine, T.W.N., 1995. Labrador Sea Water in the Eastern North Atlantic. Part I: A Synoptic Circulation Inferred from a Minimum in Potential Vorticity. *Journal of Physical Oceanography*, 25(4), 649-665.

Dan, K., Clark, R., 2017. oce: Analysis of Oceanographic Data. https://CRAN.R-project.org/package=oce

Daniault, N., Maze, J.P., Arhan, M., 1994. Circulation and Mixing of Mediterranean Water West of the Iberian Peninsula. *Deep-Sea Research Part I-Oceanographic Research Papers*, 41(11-12), 1685-1714.

Darelius, E., 2008. Topographic steering of dense overflows: Laboratory experiments with V-shaped ridges and canyons. *Deep Sea Research Part I: Oceanographic Research Papers*, 55(8), 1021-1034.

Darelius, E., Wåhlin, A., 2007. Downward flow of dense water leaning on a submarine ridge. *Deep Sea Research Part I: Oceanographic Research Papers*, 54(7), 1173-1188.

Davies, A.J., Guinotte, J.M., 2011. Global Habitat Suitability for Framework-Forming Cold-Water Corals. *PLoS ONE*, 6(4), e18483.

Davis, J.C., 1986. *Statistical and data analysis in geology*: J. Wiley.

De Clippele, L.H., Gafeira, J., Robert, K., Hennige, S., Lavaleye, M.S., Duineveld, G.C.A., Huvenne, V.A.I., Roberts, J.M., 2016. Using novel acoustic and visual mapping tools to predict the small-scale spatial distribution of live biogenic reef framework in cold-water coral habitats. *Coral Reefs*, 1-14.

de Haas, H., Mienis, F., Frank, N., Richter, T.O., Steinacher, R., de Stigter, H., van der Land, C., van Weering, T.C.E., 2009. Morphology and sedimentology of (clustered) cold-water coral mounds at the south Rockall Trough margins, NE Atlantic Ocean. *Facies*, 55(1), 1-26.

De Mol, B., Henriet, J.-P., Canals, M., 2005. Development of coral banks in Porcupine Seabight: do they have Mediterranean ancestors? In A. Freiwald, J. Murray Roberts (Eds.), *Cold-Water Corals and Ecosystems* (pp. 515-533). Berlin Heidelberg: Springer.

De Mol, L., Van Rooij, D., Pirlet, H., Greinert, J., Frank, N., Quemmerais, F., Henriet, J.P., 2011. Cold-water coral habitats in the Penmarc'h and Guilvinec Canyons (Bay of Biscay): Deep-water versus shallow-water settings. *Marine Geology*, 282(1-2), 40-52.

de Stigter, H.C., Boer, W., de Jesus Mendes, P.A., Jesus, C.C., Thomsen, L., van den Bergh, G.D., van Weering, T.C.E., 2007. Recent sediment transport and deposition in the Nazaré Canyon, Portuguese continental margin. *Marine Geology*, 246(2-4), 144-164.

Delivet, S., Van Eetvelt, B., Monteys, X., Ribó, M., Van Rooij, D., 2016. Seismic geomorphological reconstructions of Plio-Pleistocene bottom current variability at Goban Spur. *Marine Geology*, 378, 261-275.

Diaz del Rio, G., González, N., Marcote, D., 1998. The intermediate Mediterranean water inflow along the northern slope of the Iberian Peninsula. *Oceanologica Acta*, 21(2), 157-163.

Dorschel, B., Hebbeln, D., Foubert, A., White, M., Wheeler, A.J., 2007. Hydrodynamics and cold-water coral facies distribution related to recent sedimentary processes at Galway Mound west of Ireland. *Marine Geology*, 244(1-4), 184-195.

Dorschel, B., Hebbeln, D., Rüggeberg, A., Dullo, C., Freiwald, A., 2005. Growth and erosion of a cold-water coral covered carbonate mound in the Northeast Atlantic during the Late Pleistocene and Holocene. *Earth and Planetary Science Letters*, 233, 33-44.

Douarin, M., Sinclair, D.J., Elliot, M., Henry, L.-A., Long, D., Mitchison, F., Roberts, J.M., 2014. Changes in fossil assemblage in sediment cores from Mingulay Reef Complex (NE Atlantic): Implications for coral reef build-up. *Deep Sea Research Part II: Topical Studies in Oceanography*, 99, 286-296.

Duineveld, G.C., Lavaleye, M.S., Bergman, M.J., De Stigter, H., Mienis, F., 2007. Trophic structure of a cold-water coral mound community (Rockall Bank, NE Atlantic) in relation to the near-bottom particle supply and current regime. *Bulletin of Marine Science*, 81(3), 449-467.

Duineveld, G.C.A., Lavaleye, M.S.S., Berghuis, E.M., 2004. Particle flux and food supply to a seamount cold-water coral community (Galicia Bank, NW Spain). *Marine Ecology Progress Series*, 277, 13-23.

Dullo, C., Flögel, S., Rüggeberg, A., 2008. Cold-water coral growth in relation to the hydrography of the Celtic and Nordic European continental margin. *Marine Ecology Progress Series*, 371, 165-176.

Dutton, A., Lambeck, K., 2012. Ice volume and sea level during the last interglacial. *Science*, 337(6091), 216-219.

Eisele, M., Frank, N., Wienberg, C., Titschack, J., Mienis, F., Beuck, L., Tisnerat-Laborde, N., Hebbeln, D., 2014. Sedimentation patterns on a cold-water coral mound off Mauritania. *Deep Sea Research Part II: Topical Studies in Oceanography*, 99, 307-315.

Ercilla, G., Garcia-Gil, S., Estrada, F., Gracia, E., Vizcaino, A., Vaquez, J.T., Diaz, S., Vilas, F., Casas, D., Alonso, B., Danobeitia, J., Farran, M., 2008. High-resolution seismic stratigraphy of the Galicia Bank Region and neighbouring abyssal plains (NW Iberian continental margin). *Marine Geology*, 249(1-2), 108-127.

Faugères, J.-C., Gonthier, E., Mulder, T., Kenyon, N.H., Cirac, P., Griboulard, R., Berné, S., Lesuavé, R., 2002. Multi-process generated sediment waves on the Landes Plateau (Bay of Biscay, North Atlantic). *Marine Geology*, 182, 279-302.

Faugères, J.-C., Stow, D.A.V., Imbert, P., Viana, A.R., 1999. Seismic features diagnostic of contourite drifts. *Marine Geology*, 162, 1-38.

Fiúza, A.F.G., Hamann, M., Ambar, I., Díaz del Río, G., González, N., Cabanas, J.M., 1998. Water masses and their circulation off western Iberia during May 1993. *Deep Sea Research Part I: Oceanographic Research Papers*, 45(7), 1127-1160.

Flach, E., Muthumbi, A., Heip, C., 2002. Meiofauna and macrofauna community structure in relation to sediment composition at the Iberian margin compared to the Goban Spur (NE Atlantic). *Progress In Oceanography*, 52(2), 433-457.

Flögel, S., Dullo, W.C., Pfannkuche, O., Kiriakoulakis, K., Rüggeberg, A., 2014. Geochemical and physical constraints for the occurrence of living cold-water corals. *Deep Sea Research Part II: Topical Studies in Oceanography*, 99, 19-26.

Foubert, A., Huvenne, V.A.I., Wheeler, A., Kozachenko, M., Opderbecke, J., Henriet, J.P., 2011. The Moira Mounds, small cold-water coral mounds in the Porcupine Seabight, NE Atlantic: Part B--Evaluating the impact of sediment dynamics through high-resolution ROV-borne bathymetric mapping. *Marine Geology*, 282(1-2), 65-78.

Freiwald, A., Beuck, L., Rueggeberg, A., Taviani, M., Hebbeln, D., 2009. The WHITE CORAL COMMUNITY in the Central Mediterranean Sea Revealed by ROV Surveys. *Oceanography*, 22(1), 58-74.

Freiwald, A., Fossa, J.H., Grehan, A., Koslow, T., Roberts, J.M., 2004. *Cold-water coral reefs*. Cambridge: UNEP-WCMC.

Friedman, G.M., Carson, B., Ritger, S., Suess, E., 1988. Methane-derived authigenic carbonates formed by subduction-induced pore-water expulsion along the Oregon/Washington margin: Discussion and reply. *Geological Society of America Bulletin*, 100(4), 622-623.

Friocourt, Y., Blanke, B., Drijfhout, S., Speich, S., 2008. On the Dynamics of the Slope Current System along the West European Margin. Part II: Analytical Calculations and Numerical Simulations with Seasonal Forcing. *Journal of Physical Oceanography*, 38(12), 2619-2638.

Friocourt, Y., Levier, B., Speich, S., Blanke, B., Drijfhout, S.S., 2007. A regional numerical ocean model of the circulation in the Bay of Biscay. *Journal of Geophysical Research-Oceans*, 112(C9).

Gafeira, J., Diaz-Doce, D., Long, D., 2015. Semi-automated Mapping and Characterisation of Coral Reef Mounds: Mingulay Reef Proof of Concept. *British Geological Survey Internal Report*, IR/15/042, 21.

García-Lafuente, J., Díaz del Río, G., Sánchez Berrocal, C., 2006. Vertical structure and bottom-intensification of tidal currents off Northwestern Spain. *Journal of Marine Systems*, 62(1-2), 55-70.

García Lafuente, J., Garrido, J.C.S., Díaz del Río, G., Aldeanueva, F.C., Marcote, D., Sánchez Román, A., 2008. Low-frequency variability of the Mediterranean undercurrent off Galicia, northwestern Iberian Peninsula. *Journal of Marine Systems*, 74(1-2), 351-363.

Gaudin, M., Mulder, T., Cirac, P., Berne, S., Imbert, P., 2006. Past and present sedimentary activity in the Capbreton Canyon, southern Bay of Biscay. *Geo-Marine Letters*, 26(6), 331-345.

Gonthier, E., Cirac, P., Faugeres, J., Gaudin, M., Cremer, M., Bourillet, J.-F., 2006. Instabilities and deformation in the sedimentary cover on the upper slope of the southern Aquitaine continental margin, north of the Capbreton canyon (Bay of Biscay). *Scientia Marina*, 70(1), 89-100.

Greinert, J., Bohrmann, G., Suess, E., 2001. Gas Hydrate-Associated Carbonates and Methane-Venting at Hydrate Ridge: Classification, Distribution, and Origin of Authigenic Lithologies. *Natural Gas Hydrates: Occurrence, Distribution, and Detection* (pp. 99-113): American Geophysical Union.

Hall, I.R., Schmidt, S., McCave, I.N., Reyss, J.L., 2000. Particulate matter distribution and T234h/U238 disequilibrium along the Northern Iberian Margin: implications for particulate organic carbon export. *Deep Sea Research Part I: Oceanographic Research Papers*, 47(4), 557-582.

Hanebuth, T.J.J., Zhang, W., Hofmann, A.L., Löwemark, L.A., Schwenk, T., 2015. Oceanic density fronts steering bottom-current induced sedimentation deduced from a 50 ka contourite-drift record and numerical modeling (off NW Spain). *Quaternary Science Reviews*, 112, 207-225.

Harvey, J., 1982. θ-S relationships and water masses in the eastern North Atlantic. *Deep Sea Research Part A. Oceanographic Research Papers*, 29(8), 1021-1033.

He, Y., Gao, Z., Luo, J., Luo, S., Liu, X., 2008. Characteristics of internal-wave and internal-tide deposits and their hydrocarbon potential. *Petroleum Science*, 5(1), 37-44.

Hebbeln, D., Van Rooij, D., Wienberg, C., 2016. Good neighbours shaped by vigorous currents: Cold-water coral mounds and contourites in the North Atlantic. *Marine Geology*, 378, 171-185.

Henriet, J.-P., De Mol, B., Pillen, S., Vanneste, M., Van Rooij, D., Versteeg, W., Croker, P.F., Shannon, P.M., Unnithan, V., Bouriak, S., Chachkine, P., The Porcupine-Belgica 97 Shipboard Party, 1998. Gas hydrate crystals may help build reefs. *Nature*, 391, 648-649.

Henriet, J.-P., De Mol, B., Vanneste, M., Huvenne, V., Van Rooij, D., the "Porcupine-Belgica" '97 '98 and '99 shipboard parties, 2001. Carbonate mounds and slope failures in the Porcupine Basin: a development model involving past fluid venting. In P.M. Shannon, P. Haughton, D. Corcoran (Eds.), *The Petroleum Exploration of Ireland's Offshore Basins*, Vol. 188 (pp. 375-383). London: Geological Society.

Hernández-Molina, F., Campbell, S., Badalini, G., Thompson, P., Walker, R., Soto, M., Conti, B., Preu, B., Thieblemont, A., Hyslop, L., 2017. Large bedforms on contourite terraces: Sedimentary and conceptual implications. *Geology*, 46(1), 27-30.

Hernández-Molina, F.J., Nombela, M.A., Van Rooij, D., Roson, G., Ercilla, G., Urgorri, V., Llave, E., Francés, G., De Mol, L., Alejo, I., Jane, G., Mena, A., Pérez Arlucea, M., VanReusel, A., 2010. The Ortegal spur contourite depositional dystem (Bay of Biscay): the implications of the Mediterranean Outflow Waters in sedimentary processes and cold-water coral ecosystems. *VI Simposio sobre el Margen Ibérico Atlántico (MIA09)*, Abstracts Volume, 281-284.

Hernández-Molina, F.J., Paterlini, M., Violante, R., Marshall, P., de Isasi, M., Somoza, L., Rebesco, M., 2009. Contourite depositional system on the Argentine Slope: An exceptional record of the influence of Antarctic water masses. *Geology*, 37(6), 507-510.

Hernández-Molina, F.J., Serra, N., Stow, D.A.V., Llave, E., Ercilla, G., Van Rooij, D., 2011. Along-slope oceanographic processes and sedimentary products around the Iberian margin. *Geo-Marine Letters*, 31(5-6), 315-341.

Hernández-Molina, F.J., Wåhlin, A., Bruno, M., Ercilla, G., Llave, E., Serra, N., Rosón, G., Puig, P., Rebesco, M., Van Rooij, D., Roque, D., González-Pola, C., Sánchez, F., Gómez, M., Preu, B., Schwenk, T., Hanebuth, T.J.J., Sánchez Leal, R.F., García-Lafuente, J., Brackenridge, R.E., Juan, C., Stow, D.A.V., Sánchez-González, J.M., 2016. Oceanographic processes and morphosedimentary products along the Iberian margins: A new multidisciplinary approach. *Marine Geology*, 378, 127-156.

Horwitz, E.P., Dietz, M.L., Chiarizia, R., Diamond, H., Essling, A.M., Graczyk, D., 1992. Separation and preconcentration of uranium from acidic media by extraction chromatography. *Analytica Chimica Acta*, 266(1), 25-37.

Hovland, M., 2005. Pockmark-associated coral reefs at the Kristin field off Mid-Norway. *Cold-Water Corals and Ecosystems* (pp. 623-632): Springer.

Hovland, M., Judd, A.G., 1988. *Seabed pockmarks and seepages: impact on geology, biology, and the marine environment*. London: Graham & Trotman.

Hovland, M., Risk, M., 2003. Do Norwegian deep-water coral reefs rely on seeping fluids? *Marine Geology*, 198(1-2), 83-96.

Hovland, M., Thomsen, E., 1997. Cold-water corals - Are they hydrocarbon seep related? *Marine Geology*, 137(1-2), 159-164.

Huvenne, V.A.I., Masson, D., Wheeler, A., 2009a. Sediment dynamics of a sandy contourite: the sedimentary context of the Darwin cold-water coral mounds, Northern Rockall Trough. *International Journal of Earth Sciences*, 98(4), 865-884.

Huvenne, V.A.I., Tyler, P.A., Masson, D.G., Fisher, E.H., Hauton, C., Hühnerbach, V., Le Bas, T.P., Wolff, G.A., 2011. A Picture on the Wall: Innovative Mapping Reveals Cold-Water Coral Refuge in Submarine Canyon. *PLoS ONE*, 6(12), e28755.

Huvenne, V.A.I., Van Rooij, D., De Mol, B., Thierens, M., O'Donnell, R., Foubert, A., 2009b. Sediment dynamics and palaeo-environmental context at key stages in the Challenger cold-water coral mound formation: Clues from sediment deposits at the mound base. *Deep Sea Research Part I: Oceanographic Research Papers*, 56(12), 2263-2280.

Iorga, M.C., Lozier, M.S., 1999a. Signatures of the Mediterranean outflow from a North Atlantic climatology: 1. Salinity and density fields. *Journal of Geophysical Research: Oceans*, 104(C11), 25985-26009.

Iorga, M.C., Lozier, M.S., 1999b. Signatures of the Mediterranean outflow from a North Atlantic climatology 2. Diagnostic velocity fields. *Journal of Geophysical Research-Oceans*, 104(C11), 26011-26029.

IOS, SCOR, IAPSO, 2010. *The International thermodynamic equation of seawater–2010: calculation and use of thermodynamic properties.*: UNESCO.

Jané, G., Maestro, A., Ercilla, G., López-Martínez, J., De Andrés, J.R., Casas, D., González-Aller, D., Catalán-Morollón, M., 2010. Occurrence of pockmarks on the Ortegal Spur continental margin, Northwestern Iberian Peninsula. *Marine and Petroleum Geology*, 27(7), 1551-1564.

Jari, O., Blanchet, F.G., Michael, F., Roeland, K., Pierre, L., Dan, M., Peter, R.M., Hara, R.B.O., Gavin, L.S., Peter, S., Stevens, M.H.H., Eduard, S., Helene, W., 2017. vegan: Community Ecology Package. https://CRAN.R-project.org/package=vegan

Kellogg, C.A., Lisle, J.T., Galkiewicz, J.P., 2009. Culture-independent characterization of bacterial communities associated with the cold-water coral Lophelia pertusa in the northeastern Gulf of Mexico. *Appl Environ Microbiol*, 75(8), 2294-2303.

Kiriakoulakis, K., Fisher, E., Wolff, G.A., Freiwald, A., Grehan, A., Roberts, J.M., 2005. Lipids and nitrogen isotopes of two deep-water corals from the North-East Atlantic: initial results and

implications for their nutrition. In A. Freiwald, J.M. Roberts (Eds.), *Cold-Water Corals and Ecosystems* (pp. 715-729). Berlin, Heidelberg: Springer Berlin Heidelberg.

Kissel, C., Van Toer, A., Laj, C., Cortijo, E., Michel, E., 2013. Variations in the strength of the North Atlantic bottom water during Holocene. *Earth and Planetary Science Letters*, 369, 248-259.

Knott, S.D., Burchell, M.T., Jolley, E.J., Fraser, A.J., 1993. Mesozoic to Cenozoic Plate Reconstructions of the North-Atlantic and Hydrocarbon Plays of the Atlantic Margins. *Petroleum Geology of Northwest Europe: Proceedings of the 4th Conference*, 953-974.

Lamb, K.G., 2014. Internal Wave Breaking and Dissipation Mechanisms on the Continental Slope/Shelf. In S.H. Davis, P. Moin (Eds.), *Annual Review of Fluid Mechanics, Vol 46*, Vol. 46 (pp. 231-254). Palo Alto: Annual Reviews.

Lee, I.H., Lien, R.-C., Liu, J.T., Chuang, W.-s., 2009. Turbulent mixing and internal tides in Gaoping (Kaoping) Submarine Canyon, Taiwan. *Journal of Marine Systems*, 76(4), 383-396.

Legg, S., Ezer, T., Jackson, L., Briegleb, B., Danabasoglu, G., Large, W., Wu, W., Chang, Y., Özgökmen, T.M., Peters, H., 2009. Improving oceanic overflow representation in climate models: the gravity current entrainment climate process team. *Bulletin of the American Meteorological Society*, 90(5), 657-670.

Lippold, J., Gutjahr, M., Blaser, P., Christner, E., de Carvalho Ferreira, M.L., Mulitza, S., Christl, M., Wombacher, F., Böhm, E., Antz, B., Cartapanis, O., Vogel, H., Jaccard, S.L., 2016. Deep water provenance and dynamics of the (de)glacial Atlantic meridional overturning circulation. *Earth and Planetary Science Letters*, 445, 68-78.

Llave, E., Hernández-Molina, F., Ercilla, G., Roque, C., Van Rooij, D., García, M., Juan, C., Mena, A., Brackenridge, R., Jané, G., 2015. Bottom current processes along the Iberian continental margin. *Boletín Geológico y Minero*, 126(2-3), 219-256.

Llave, E., Hernández-Molina, F.J., Somoza, L., Stow, D.A.V., Diaz del Rio, G., 2007. Quaternary evolution of the contourite depositional system in the Gulf of Cadiz. In A.R. Viana, M. Rebesco (Eds.), *Economic and Palaeoceanographic Significance of Contourite Deposits*, Vol. 276 (pp. 49-79). London: Geological Society.

Løseth, H., Gading, M., Wensaas, L., 2009. Hydrocarbon leakage interpreted on seismic data. *Marine and Petroleum Geology*, 26(7), 1304-1319.

Maestro, A., López-Martínez, J., Llave, E., Bohoyo, F., Acosta, J., Hernández-Molina, F.J., Muñoz, A., Jané, G., 2013. Geomorphology of the Iberian Continental Margin. *Geomorphology*, 196, 13-35.

Magalhães, V.H., Pinheiro, L.M., Ivanov, M.K., Kozlova, E., Blinova, V., Kolganova, J., Vasconcelos, C., McKenzie, J.A., Bernasconi, S.M., Kopf, A.J., Díaz-del-Río, V., González, F.J., Somoza, L., 2012. Formation processes of methane-derived authigenic carbonates from the Gulf of Cadiz. *Sedimentary Geology*, 243-244, 155-168.

Mazé, J.P., Arhan, M., Mercier, H., 1997. Volume budget of the eastern boundary layer off the Iberian Peninsula. *Deep Sea Research Part I: Oceanographic Research Papers*, 44(9–10), 1543-1574.

McArdle, B.H., Anderson, M.J., 2001. Fitting multivariate models to community data: a comment on distance-based redundancy analysis. *Ecology*, 82(1), 290-297.

McCave, I.N., 1982. Erosion and deposition by currents on submarine slopes. *Bull. Inst. Géol. Bassin d'Aquitaine*, 31, 47-55.

McCave, I.N., Hall, I.R., 2002. Turbidity of waters over the Northwest Iberian continental margin. *Progress In Oceanography*, 52(2–4), 299-313.

McManus, J.F., Francois, R., Gherardi, J.M., Keigwin, L.D., Brown-Leger, S., 2004. Collapse and rapid resumption of Atlantic meridional circulation linked to deglacial climate changes. *Nature*, 428(6985), 834-837.

Mienis, F., de Stigter, H., White, M., Duineveld, G.C.A., de Haas, H., van Weering, T., 2007. Hydrodynamic controls on cold-water coral growth and carbonate-mound development at the SW and SE Rockall Trough Margin, NE Atlantic Ocean. *Deep-Sea Research I*, 54, 1655-1674.

Mienis, F., De Stigter, H.C., De Haas, H., Van der Land, C., Van Weering, T.C.E., 2012a. Hydrodynamic conditions in a cold-water coral mound area on the Renard Ridge, southern Gulf of Cadiz. *Journal of Marine Systems*, 96–97(0), 61-71.

Mienis, F., de Stigter, H.C., de Haas, H., van Weering, T.C.E., 2009. Near-bed particle deposition and resuspension in a cold-water coral mound area at the Southwest Rockall Trough margin, NE Atlantic. *Deep Sea Research Part I: Oceanographic Research Papers*, 56(6), 1026-1038.

Mienis, F., Duineveld, G.C.A., Davies, A.J., Ross, S.W., Seim, H., Bane, J., van Weering, T.C.E., 2012b. The influence of near-bed hydrodynamic conditions on cold-water corals in the Viosca Knoll area, Gulf of Mexico. *Deep Sea Research Part I: Oceanographic Research Papers*, 60(0), 32-45.

Mohn, C., Rengstorf, A., White, M., Duineveld, G., Mienis, F., Soetaert, K., Grehan, A., 2014. Linking benthic hydrodynamics and cold-water coral occurrences: A high-resolution model study at three cold-water coral provinces in the NE Atlantic. *Progress In Oceanography*, 122, 92-104.

Mojtahid, M., Eynaud, F., Zaragosi, S., Scourse, J.D., Bourillet, J.F., Garlan, T., 2005. Palaeoclimatology and palaeohydrography of the glacial stages on Celtic and Armorican margins over the last 360000 yrs. *Marine Geology*, 224, 57-82.

Mulder, T., Zaragosi, S., Garlan, T., Mavel, J., Cremer, M., Sottolichio, A., Sénéchal, N., Schmidt, S., 2012. Present deep-submarine canyons activity in the Bay of Biscay (NE Atlantic). *Marine Geology*, 295–298(0), 113-127.

Oberle, F.K.J., Storlazzi, C.D., Hanebuth, T.J.J., 2016. What a drag: Quantifying the global impact of chronic bottom trawling on continental shelf sediment. *Journal of Marine Systems*, 159, 109-119.

Oliveira, A., Santos, A.I., Rodrigues, A., Vitorino, J., 2007. Sedimentary particle distribution and dynamics on the Nazaré canyon system and adjacent shelf (Portugal). *Marine Geology*, 246(2), 105-122.

Peliz, Á., Dubert, J., Santos, A.M.P., Oliveira, P.B., Le Cann, B., 2005. Winter upper ocean circulation in the Western Iberian Basin—Fronts, Eddies and Poleward Flows: an overview. *Deep Sea Research Part I: Oceanographic Research Papers*, 52(4), 621-646.

Pichon, A., Morel, Y., Baraille, R., Quaresma, L.S., 2013. Internal tide interactions in the Bay of Biscay: Observations and modelling. *Journal of Marine Systems*, 109-110, S26-S44.

Pilcher, R., Argent, J., 2007. Mega-pockmarks and linear pockmark trains on the West African continental margin. *Marine Geology*, 244, 15-32.

Pingree, R.D., Le Cann, B., 1990. Structure, strength and seasonality of the slope currents in the Bay of Biscay region. *Journal of the Marine Biological Association of the United Kingdom*, 70, 857-885.

Pollard, S., Griffiths, C.R., Cunningham, S.A., Read, J.F., Perez, F.F., Ríos, A.F., 1996. Vivaldi 1991 - A study of the formation, circulation and ventilation of Eastern North Atlantic Central Water. *Progress In Oceanography*, 37, 167-192.

Pomar, L., Morsilli, M., Hallock, P., Bádenas, B., 2012. Internal waves, an under-explored source of turbulence events in the sedimentary record. *Earth-Science Reviews*, 111(1–2), 56-81.

Pons-Branchu, E., Douville, E., Roy-Barman, M., Dumont, E., Branchu, P., Thil, F., Frank, N., Bordier, L., Borst, W., 2014. A geochemical perspective on Parisian urban history based on U–Th dating, laminae counting and yttrium and REE concentrations of recent carbonates in underground aqueducts. *Quaternary Geochronology*, 24, 44-53.

Preu, B., Hernández-Molina, F.J., Violante, R., Piola, A.R., Paterlini, C.M., Schwenk, T., Voigt, I., Krastel, S., Spiess, V., 2013. Morphosedimentary and hydrographic features of the northern Argentine margin: The interplay between erosive, depositional and gravitational processes and its conceptual implications. *Deep-Sea Research Part I-Oceanographic Research Papers*, 75, 157-174.

Price, J.F., Baringer, O.N.M., 1994. Outflows and deep water production by marginal seas. *Progress In Oceanography*, 33(3), 161-200.

Prieto, E., González-Pola, C., Lavín, A., Sánchez, R., Ruiz-Villarreal, M., 2013. Seasonality of intermediate waters hydrography west of the Iberian Peninsula from an 8 yr semiannual time series of an oceanographic section. *Ocean Sci.*, 9(2), 411-429.

Puig, P., Palanques, A., Martín, J., 2014. Contemporary sediment-transport processes in submarine canyons. *Annual review of marine science*, 6, 53-77.

RCoreTeam, 2015. R: A Language and Environment for Statistical Computing.

Rebesco, M., Camerlenghi, A., (Eds.), 2008. *Contourites*: Elsevier.

Rebesco, M., Hernández-Molina, F.J., Van Rooij, D., Wåhlin, A., 2014. Contourites and associated sediments controlled by deep-water circulation processes: State-of-the-art and future considerations. *Marine Geology*, 352, 111-154.

Reeder, D.B., Ma, B.B., Yang, Y.J., 2011. Very large subaqueous sand dunes on the upper continental slope in the South China Sea generated by episodic, shoaling deep-water internal solitary waves. *Marine Geology*, 279(1-4), 12-18.

Ribó, M., Puig, P., Muñoz, A., Lo Iacono, C., Masqué, P., Palanques, A., Acosta, J., Guillén, J., Gómez Ballesteros, M., 2016. Morphobathymetric analysis of the large fine-grained sediment waves over the Gulf of Valencia continental slope (NW Mediterranean). *Geomorphology*, 253, 22-37.

Roberts, J.M., Wheeler, A.J., Freiwald, A., 2006. Reefs of the Deep: The Biology and Geology of Cold-Water Coral Ecosystems. *Science*, 312(5773), 543-547.

Rogers, A.D., 1999. The biology of *Lophelia pertusa* (LINNAEUS 1758) and other deep-water reef-forming corals and impacts from human activities. *International Reviews of Hydrobiology*, 84(4), 315-406.

Rogerson, M., Bigg, G.R., Rohling, E.J., Ramirez, J., 2011. Vertical density gradient in the eastern North Atlantic during the last 30,000 years. *Climate Dynamics*, 39(3-4), 589-598.

Rogerson, M., Rohling, E., Bigg, G.R., Ramirez, J., 2012. Paleoceanography of the Atlantic-Mediterranean exchange: Overview and first quantitative assessment of climatic forcing. *Reviews of Geophysics*, 50(2).

Roquet, F., Madec, G., McDougall, T.J., Barker, P.M., 2015. Accurate polynomial expressions for the density and specific volume of seawater using the TEOS-10 standard. *Ocean Modelling*, 90(Supplement C), 29-43.

Rüggeberg, A., Flögel, S., Dullo, W.C., Raddatz, J., Liebetrau, V., 2016. Paleo-seawater density reconstruction and its implication for cold-water coral carbonate mounds in the northeast Atlantic through time. *Paleoceanography*, 31(3), 365-379.

Salgueiro, E., Voelker, A., Abrantes, F., Meggers, H., Pflaumann, U., Lončarić, N., González-Álvarez, R., Oliveira, P., Bartels-Jónsdóttir, H.B., Moreno, J., Wefer, G., 2008. Planktonic foraminifera from modern sediments reflect upwelling patterns off Iberia: Insights from a regional transfer function. *Marine Micropaleontology*, 66(3), 135-164.

Sánchez, F., González-Pola, C., Druet, M., García-Alegre, A., Acosta, J., Cristobo, J., Parra, S., Ríos, P., Altuna, Á., Gómez-Ballesteros, M., Muñoz-Recio, A., Rivera, J., del Río, G.D., 2014. Habitat characterization of deep-water coral reefs in La Gaviera Canyon (Avilés Canyon System, Cantabrian Sea). *Deep Sea Research Part II: Topical Studies in Oceanography*, 106, 118-140.

Schönfeld, J., Zahn, R., 2000. Late Glacial to Holocene history of the Mediteranean Outflow. Evidence from benthic foraminiferal assemblages and stable isotopes at the Portuguese margin. *Palaeogeography, Palaeoclimatology, Palaeoecology*, 159, 85-111.

Shanmugam, G., 2003. Deep-marine tidal bottom currents and their reworked sands in modern and ancient submarine canyons. *Marine and Petroleum Geology*, 20, 471-491.

Shepard, F.P., 1975. Progress of internal waves along submarine canyons. *Marine Geology*, 19(3), 131-138.

Somoza, L., Ercilla, G., Urgorri, V., León, R., Medialdea, T., Paredes, M., Gonzalez, F.J., Nombela, M.A., 2014. Detection and mapping of cold-water coral mounds and living Lophelia reefs in the Galicia Bank, Atlantic NW Iberia margin. *Marine Geology*, 349, 73-90.

Stewart, H., Davies, J., 2007. SW approaches MESH survey, R/V Celtic Explorer cruise CE0705, BGS project 2007/06 : operations report. (p. 88): Mapping European Seabed Habitats (MESH).

Stewart, H.A., Davies, J.S., Guinan, J., Howell, K.L., 2014. The Dangeard and Explorer canyons, South Western Approaches UK: Geology, sedimentology and newly discovered cold-water coral mini-mounds. *Deep Sea Research Part II: Topical Studies in Oceanography*, 104(0), 230-244.

Stow, D.A.V., Faugères, J.-C., Howe, J.A., Pudsey, C.J., Viana, A.R., 2002. Bottom currents, contourites and deep-sea sediment drifts: current state-of-the-art. In D.A.V. Stow, C.J. Pudsey, J.A. Howe, J.-C. Faugères, A.R. Viana (Eds.), *Deep-Water Contourite Systems: Modern Drifts and Ancient Series, Seismic and Sedimentary Characteristics*, Vol. 22 (pp. 7-20). London: Geological Society.

Stow, D.A.V., Hernández-Molina, F.J., Llave, E., Sayago-Gil, M., del Rio, V.D., Branson, A., 2009. Bedform-velocity matrix: The estimation of bottom current velocity from bedform observations. *Geology*, 37(4), 327-330.

Talley, L.D., McCartney, M.S., 1982. Distribution and Circulation of Labrador Sea Water. *Journal of Physical Oceanography*, 12(11), 1189-1205.

Thornalley, D.J., Blaschek, M., Davies, F.J., Praetorius, S., Oppo, D.W., McManus, J.F., Hall, I.R., Kleiven, H., Renssen, H., McCave, I.N., 2013. Long-term variations in Iceland–Scotland overflow strength during the Holocene. *Climate of the Past*, 9(5), 2073-2084.

Van Aken, H.M., 2000. The hydrography of the mid-latitude Northeast Atlantic Ocean II: The intermediate water masses. *Deep-Sea Research I*, 47, 789-824.

van de Flierdt, T., Robinson, L.F., Adkins, J.F., 2010. Deep-sea coral aragonite as a recorder for the neodymium isotopic composition of seawater. *Geochimica et Cosmochimica Acta*, 74(21), 6014-6032.

van Haren, H., Mienis, F., Duineveld, G.C.A., Lavaleye, M.S.S., 2014. High-resolution temperature observations of a trapped nonlinear diurnal tide influencing cold-water corals on the Logachev mounds. *Progress In Oceanography*, 125, 16-25.

Van Rooij, D., Huvenne, V.A.I., Blamart, D., Henriet, J.P., Wheeler, A., de Haas, H., 2009. The Enya mounds: a lost mound-drift competition. *International Journal of Earth Sciences*, 98(4), 849-863.

van Weering, T.C.E., de Stigter, H.C., Boer, W., de Haas, H., 2002. Recent sediment transport and accumulation on the NW Iberian margin. *Progress In Oceanography*, 52(2), 349-371.

Varela, R.A., Rosón, G., Herrera, J.L., Torres-López, S., Fernández-Romero, A., 2005. A general view of the hydrographic and dynamical patterns of the Rías Baixas adjacent sea area. *Journal of Marine Systems*, 54(1–4), 97-113.

Victorero, L., Blamart, D., Pons-Branchu, E., Mavrogordato, M.N., Huvenne, V.A.I., 2016. Reconstruction of the formation history of the Darwin Mounds, N Rockall Trough: How the dynamics of a sandy contourite affected cold-water coral growth. *Marine Geology*, 378, 186-195.

Vlasenko, V., Stashchuk, N., Inall, M.E., Hopkins, J.E., 2014. Tidal energy conversion in a global hot spot: On the 3-D dynamics of baroclinic tides at the Celtic Sea shelf break. *Journal of Geophysical Research: Oceans*, 119(6), 3249-3265.

Vlasenko, V., Stashchuk, N., Inall, M.E., Porter, M., Aleynik, D., 2016. Focusing of baroclinic tidal energy in a canyon. *Journal of Geophysical Research: Oceans*, 121(4), 2824-2840.

Wåhlin, A.K., Walin, G., 2001. Downward Migration of Dense Bottom Currents. *Environmental Fluid Mechanics*, 1(2), 257-279.

Weaver, P.P.E., Wynn, R.B., Kenyon, N.H., Evans, J., 2000. Continental margin sedimentation, with special reference to the north-east Atlantic margin. *Sedimentology*, 47(Suppl. 1), 239-256.

Wehrmann, L.M., Templer, S.P., Brunner, B., Bernasconi, S.M., Maignien, L., Ferdelman, T.G., 2011. The imprint of methane seepage on the geochemical record and early diagenetic processes in cold-water coral mounds on Pen Duick Escarpment, Gulf of Cadiz. *Marine Geology*, 282(1-2), 118-137.

Weiss, A.D., 2001. Topographic Positions and Landforms Analysis (poster). *ESRI International User Conference*.

Wheeler, A.J., Beyer, A., Freiwald, A., de Haas, H., Huvenne, V.A.I., Kozachenko, M., Olu-Le Roy, K., Opderbecke, J., 2007. Morphology and environment of cold-water coral carbonate mounds on the NW European margin. *International Journal of Earth Sciences*, 96, 37-56.

Wheeler, A.J., Kozachenko, M., Henry, L.A., Foubert, A., de Haas, H., Huvenne, V.A.I., Masson, D.G., Olu, K., 2011. The Moira Mounds, small cold-water coral banks in the Porcupine Seabight, NE Atlantic: Part A--an early stage growth phase for future coral carbonate mounds? *Marine Geology*, 282(1-2), 53-64.

White, M., 2007. Benthic dynamics at the carbonate mound regions of the Porcupine Sea Bight continental margin. *International Journal of Earth Sciences*, 96, 1-9.

White, M., Dorschel, B., 2010. The importance of the permanent thermocline to the cold water coral carbonate mound distribution in the NE Atlantic. *Earth and Planetary Science Letters*, 296(3-4), 395-402.

White, M., Mohn, C., de Stigter, H., Mottram, G., 2005. Deep-water coral development as a function of hydrodynamics and surface productivity around the submarine banks of the Rockall Trough, NE Atlantic. *Cold-Water Corals and Ecosystems*, 503-514.

Williams, C.A., 1975. Sea-Floor Spreading in Bay of Biscay and Its Relationship to North-Atlantic. *Earth and Planetary Science Letters*, 24(3), 440-456.

Wright, D., Pendleton, M., Boulware, J., Walbridge, S., Gerlt, B., Eslinger, D., Sampson, D., Huntley, E., 2012. ArcGIS Benthic Terrain Modeler (BTM), v. 3.0, Environmental Systems Research Institute, NOAA Coastal Services Center, Massachusetts Office of Coastal Zone Management. *esriurl. com/5754*.

Wynn, R., Masson, D., 2008. Sediment waves and bedforms. *Developments in sedimentology*, 60, 289-300.

Zhang, H., King, B., Swinney, H.L., 2008. Resonant generation of internal waves on a model continental slope. *Physical Review Letters*, 100(24), 244504.

Figure 1: Location of the study area on the outer Ortegal Spur and Ferrol Canyon head at the NW Iberian margin. Contour lines are drawn at 100 m interval. (A) Geological map modified from Lamboy and Dupeuble (1975) with the tectonic setting modified from Boillot and Malod (1988). The dotted lines represent the canyon axes after Maestro et al. (2013). (B) Main water masses and circulation pattern in the upper 1500 m of the water column: MOW = Mediterranean Outflow Water, modified from Iorga and Lozier (1999a); ENACWst = subtropical Eastern North Atlantic Central Water; ENACWsp = subpolar Eastern North Atlantic Central Water; PC = Portugal Current; PCC = Portugal Coastal Current; IPCs = Iberian Poleward Current system and Finisterre Front modified from Varela et al. (2005).

Figure 2: Multibeam bathymetry map of the study area with locations of the reflection seismic profiles, ROV dives, CTD casts and references to figures.

Figure 3: (A) Mosaic of high resolution multibeam backscatter intensities; (B) geomorphologic analysis of the study area; basement structures and faults were modified from Boillot and Malod (1988).

Figure 4: Sparker reflection seismic profiles (for locations see Fig. 2). (A) N-S profile over the contourite terrace with an associated plastered drift and a moat at its lower edge. The acoustic basement (AB) is affected by several normal faults forming a horst structure and a tilted block. (B) W-E profile over the contourite terrace, erosional surface and abraded surface incised by several furrows. (C) W-E profile over the contourite terrace, erosional surface and mounded elongated and separated drift with associated moat. Hydrographic panels are based on WOD13 CTD data collected between March and May (1990-1996) and two CTD casts collected in May 2009: Practical Salinity (colour shading) and Temperature in °C (contours). ENACW = Eastern North Atlantic Central Water; MOW= Mediterranean Outflow Water.

Figure 5: Seismic anomalies related to fluid migration (for locations see Fig. 2): (A) Large pockmark and elevated rim with an underlying vertical wipe out zone, bright spots and vertical dim zones. (B) Pockmark with an associated wipe out zone, intra-sedimentary doming and vertical dim zones. (C) Mini-mounds on the Ortegal Spur terrace to the south of the Ferrol Canyon head. Left mini-mound positioned above reflection pull-up, dim spots, vertical discontinuity and dim zones.

Figure 6: ROV observations over the mini-mounds: (A) Example image of mound facies: bioturbated seafloor with mixed bioclastic and siliciclastic sands with buried *L. pertusa* framework and scattered coral rubble; (B) Example image of off-mound facies: bioturbated seafloor with mixed bioclastic and siliciclastic sands. (C) Detailed hill shaded bathymetry map of identified mini-mounds (for location see Fig. 2) with mapped feature outline, seafloor facies interpretations documented in (A) and (B) and location of the *L. pertusa* sample ; (D) Detailed backscatter intensity map.

Figure 7: Scatterplot of the principal components (A) PC1 vs. PC2 and (B) PC1 vs. PC3. Ellipses contain 95% of data points of each group. Red arrows represent the loadings of the different morphological characteristics on each of the principal components: mean_diam = mean diameter, nn_dist = nearest neighbor distance, w_l_ratio = width to length ratio, azimuth = the azimuth of the long axis.

Figure 8: (A) Salinity and temperature profile of CTD1 (full line) and CTD 2 (dashed line; for location see Fig. 2) with indication of the water masses: ENACW = Eastern North Atlantic Central Water; MOW = Mediterranean Outflow Water. (B) Θ-S plot of CTD1 with potential density contours. The black lines indicate mixing triangles and the blue dots represent reference points for the different water mass end-members: (1) lower end of ENACW of subtropical origin (Harvey, 1982); (2) lower end of ENACW of sub polar origin (Castro et al., 1998); (3) lower core of MOW in Cape St-Vincent (Ambar and Howe, 1979); (4) Labrador Sea Water (LSW) (Cunningham and Haine, 1995; Talley and McCartney, 1982). (C) Potential density σ_θ and buoyancy frequency N profile of CTD1 (full line) and CTD2 (dashed line). The vertical blue box indicates the potential density range σ_θ

=27.35-27.65 kg/m^3. (D) Map of the M2 internal tide reflection condition γ/c with γ the slope of the topography and c the characteristic angle of the incoming internal tides. The dark grey zones represent the MOW core where the fraction of (3) is greater than 40%. The light grey zones represents the ENACW-MOW mixing zone where the fraction of (3) is between 20% and 40%. The yellow zones corresponds to the depth interval of the mini-mounds.

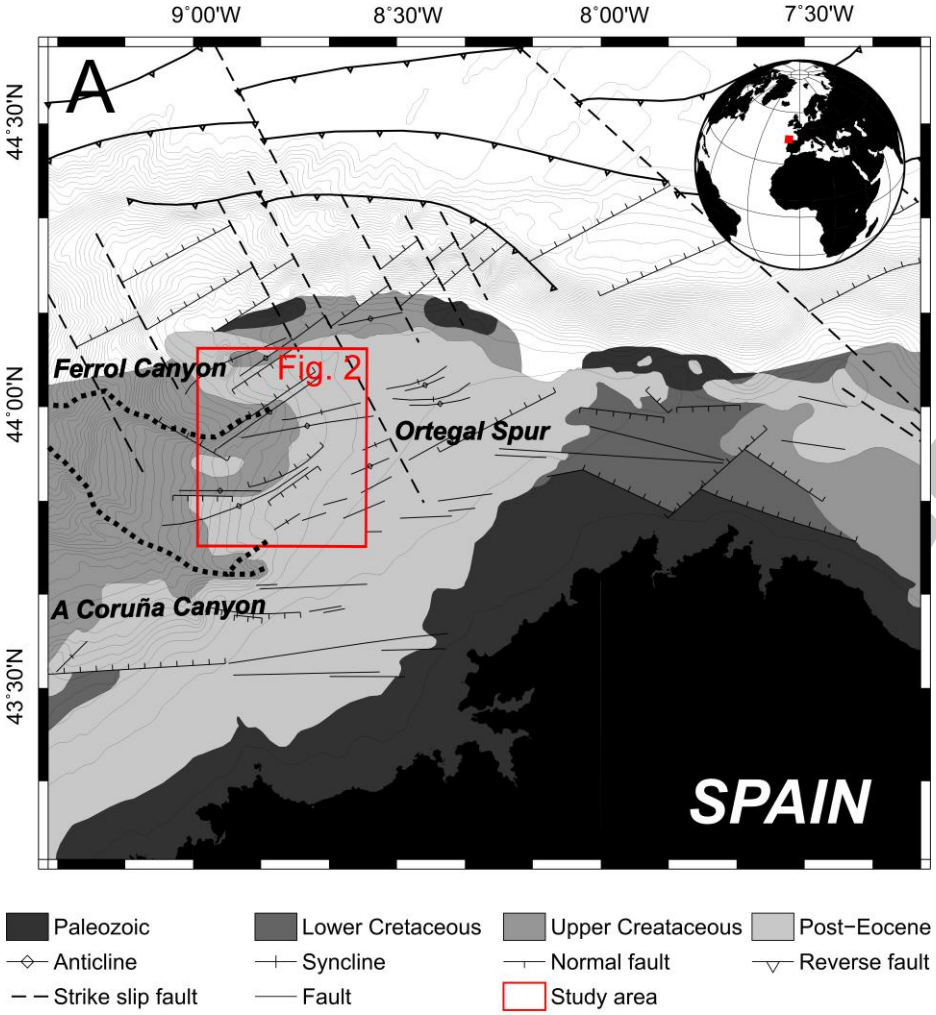

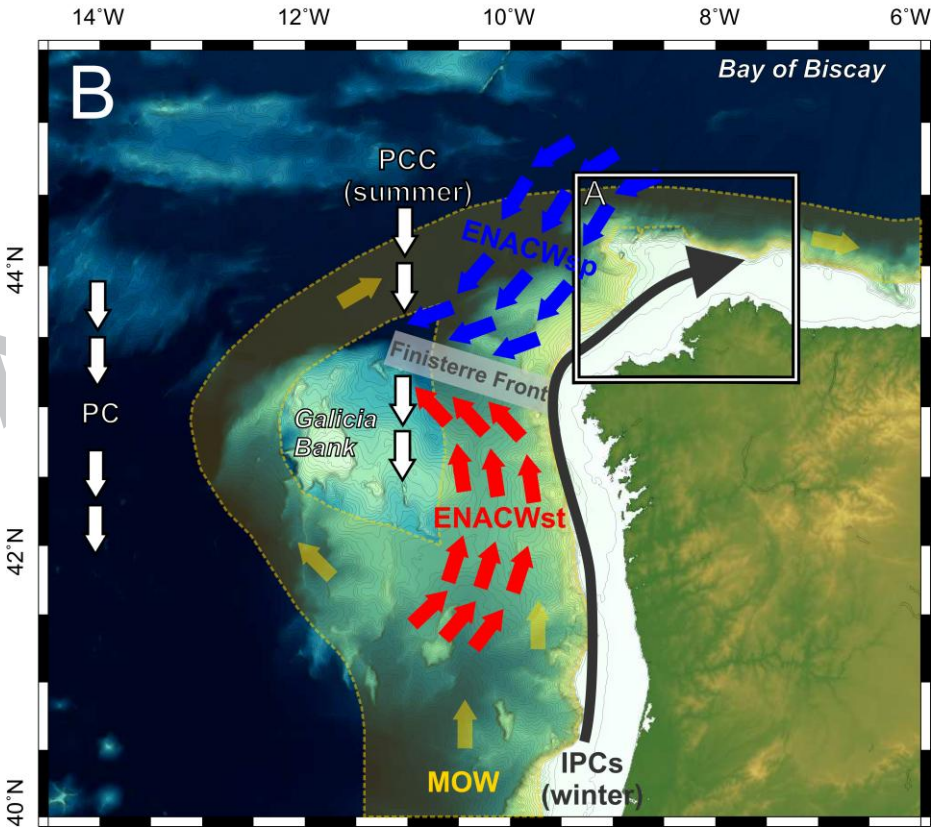

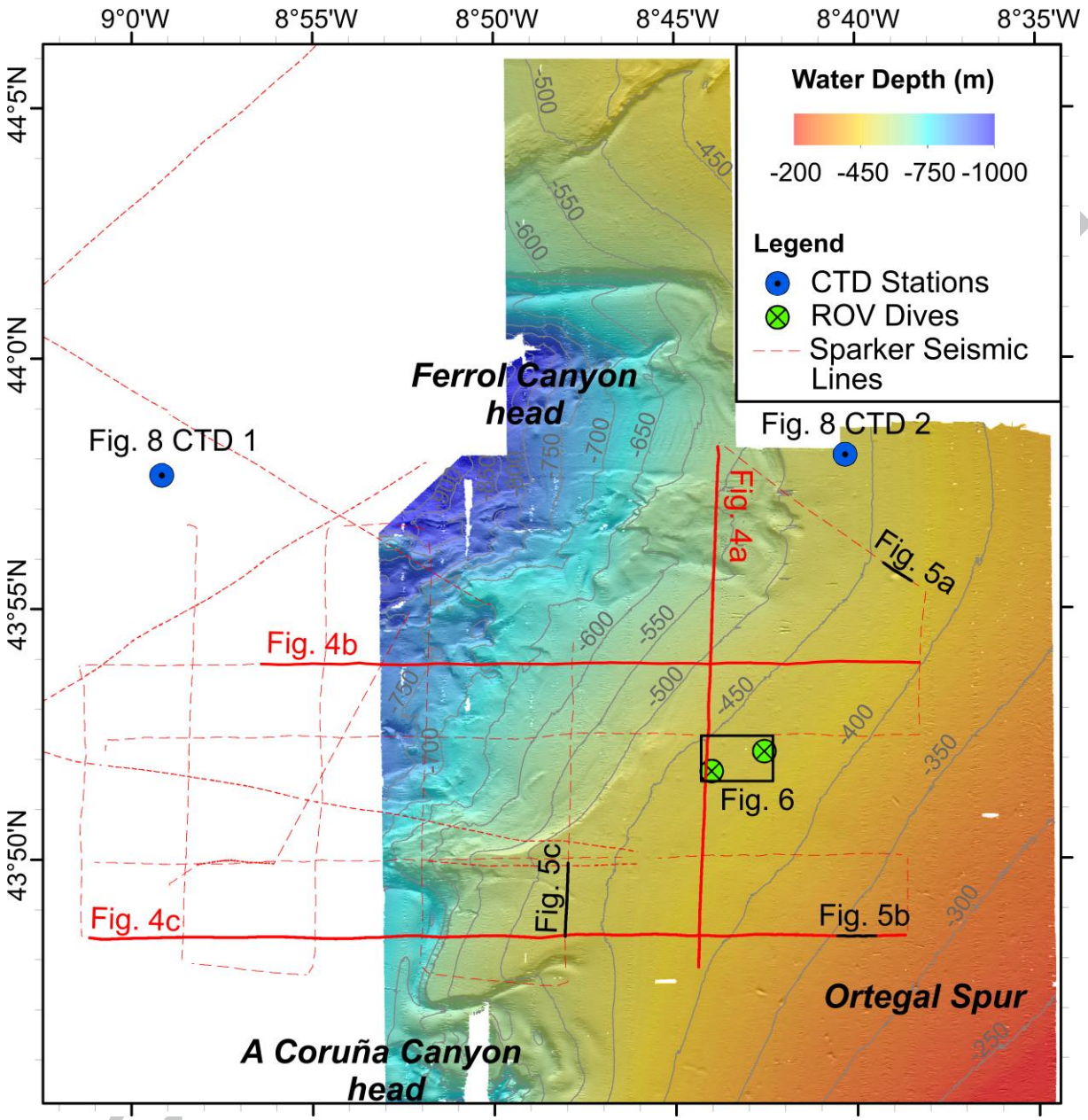

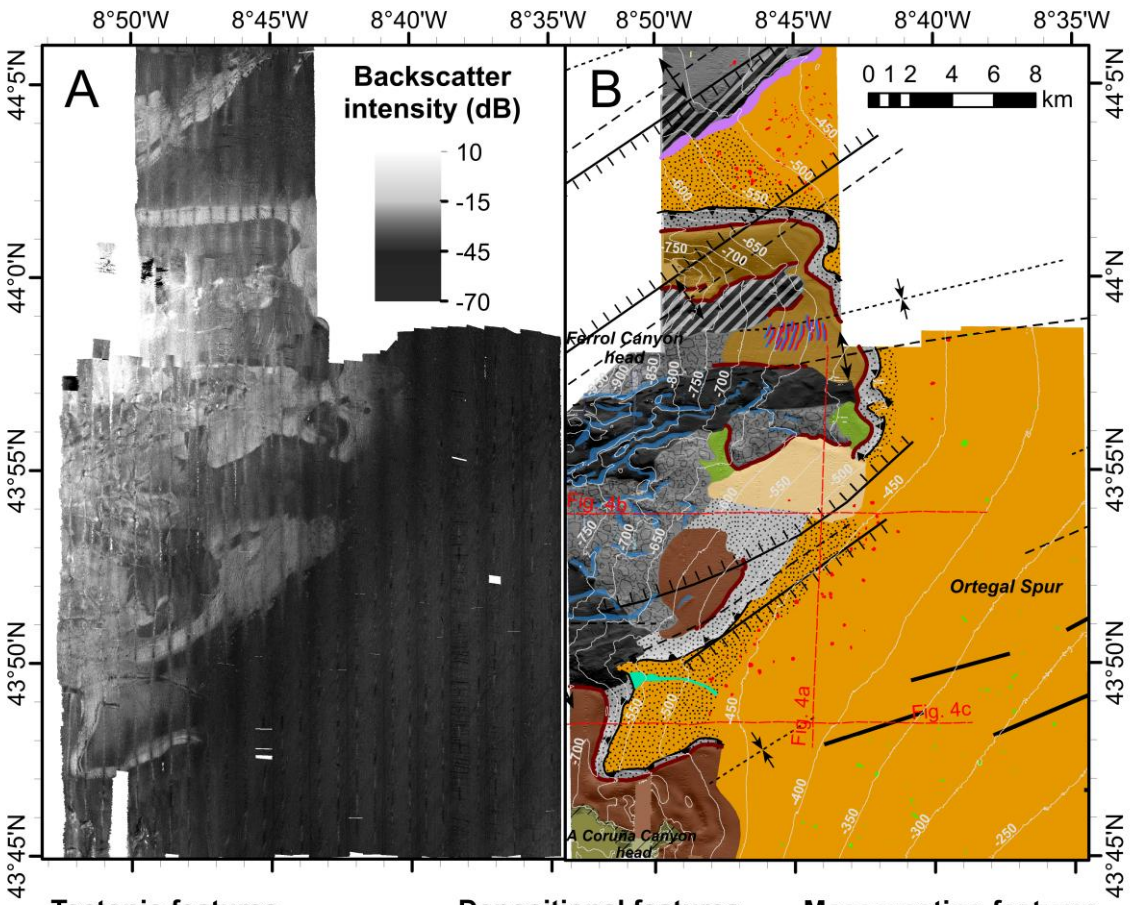

Tectonic features
- Syncline
- Anticline
- Fault
- Normal faults
- Acoustic basement outcrop
- (Undefined) basement outcrop

Erosional features
- Erosional surface
- Abraded surface
- Escarpment
- Contourite channel (moat)
- Channel
- Furrow
- Blind canyon

Depositional features

Contourite drifts
- Mounded confined drift
- Plastered drift
- Mounded patch drift
- Mounded separated drift

Sediment Waves
- Wave crest
- Wave trough

Mixed erosional-depositional features

Contourite terrace
- Depositional
- Erosional

Mass wasting features
- Slide scar
- Slump

Fluid migration features
- Pockmarks

Biogenic features
- Mini-mounds

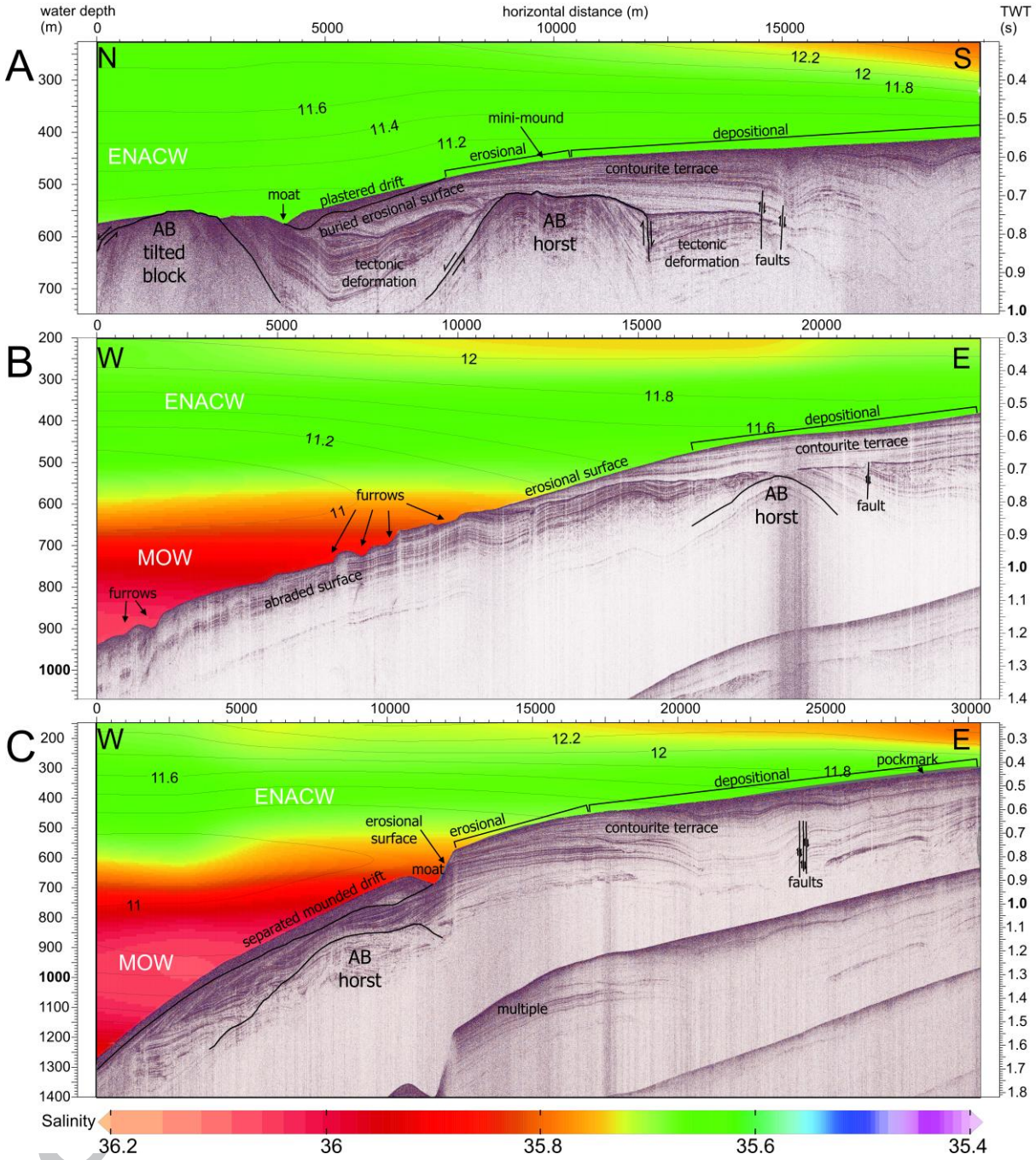

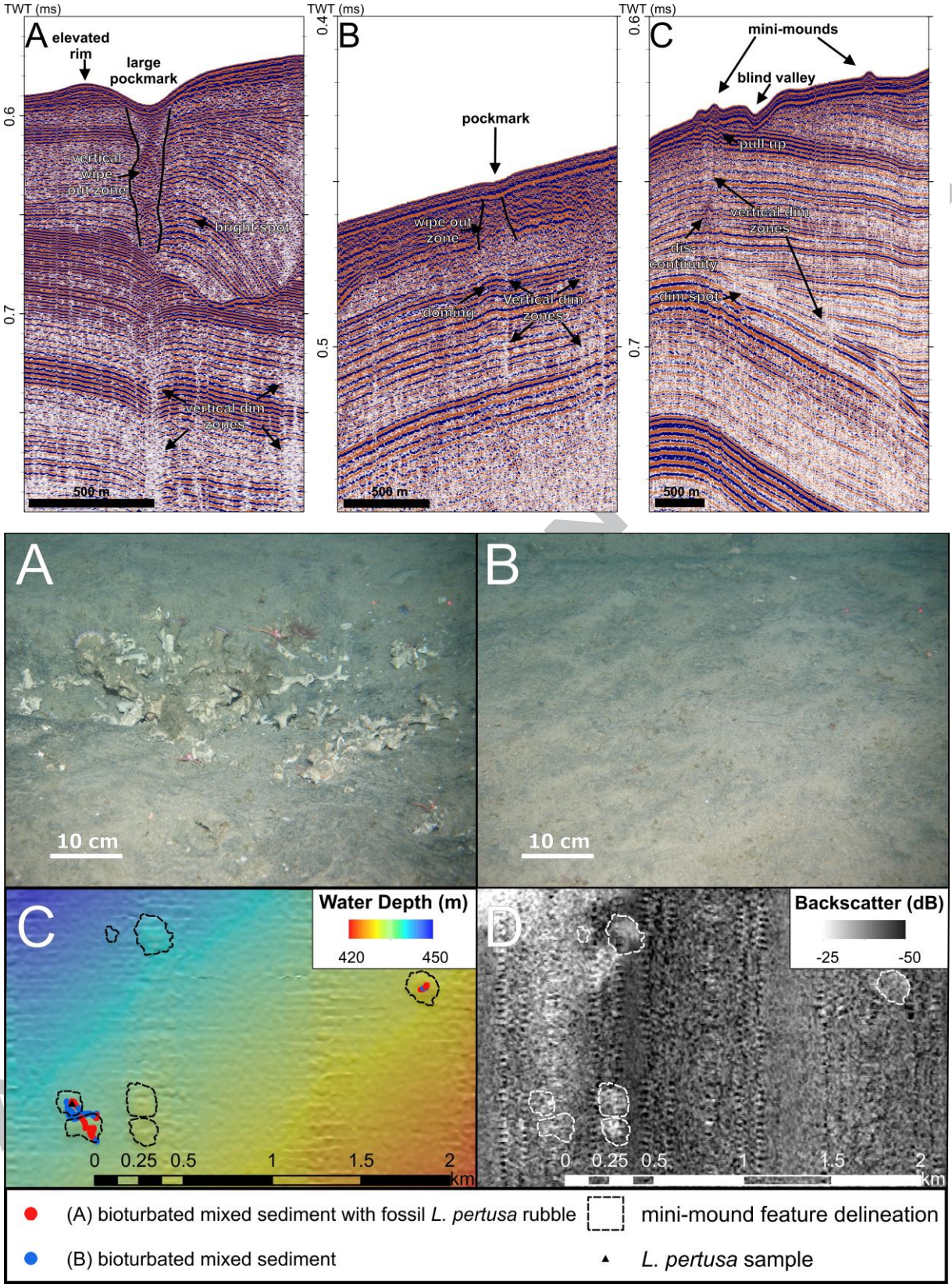

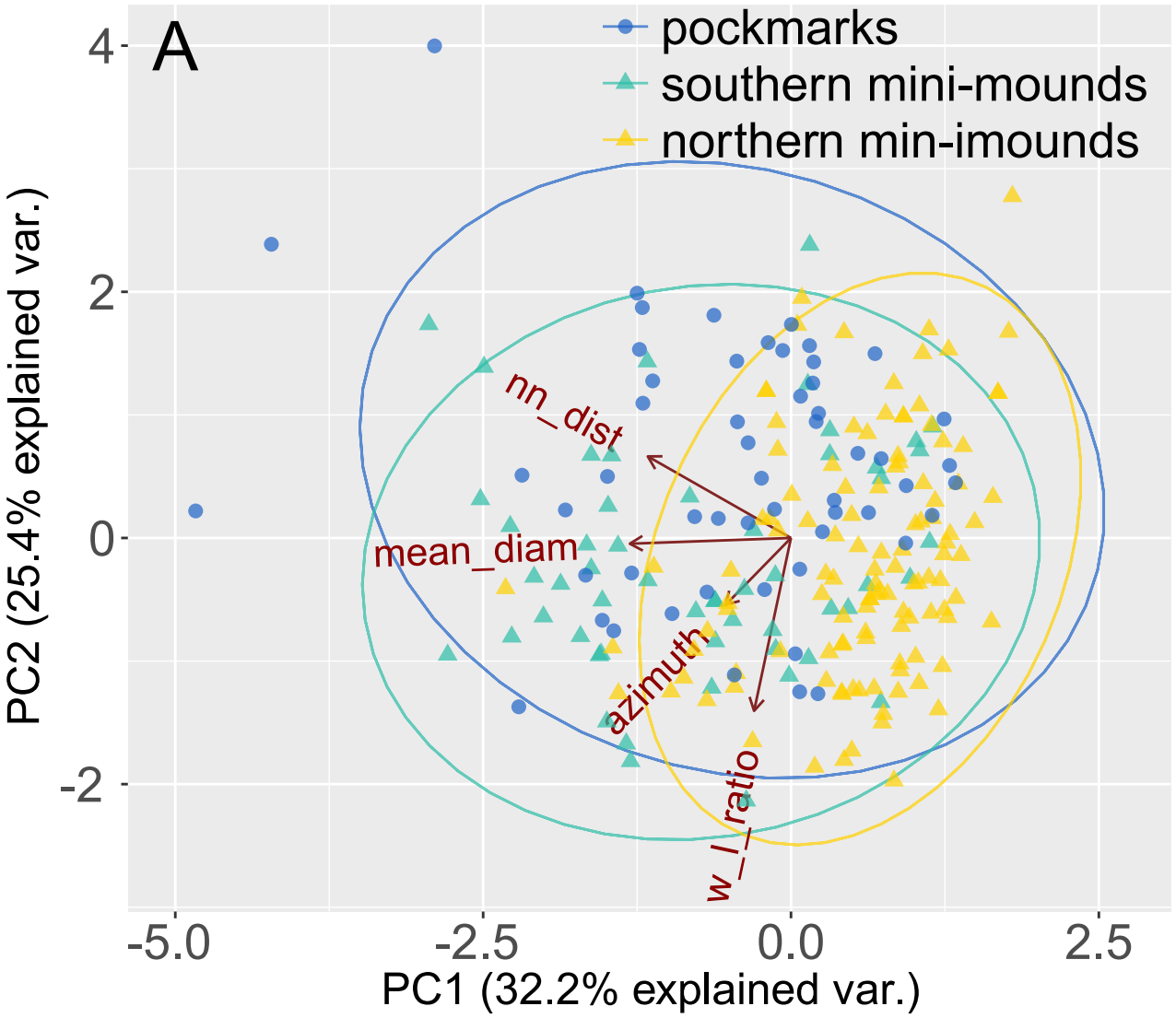
A
pockmarks
southern mini-mounds
northern min-imounds
nn_dist
mean_diam
azimuth
w_l_ratio
PC2 (25.4% explained var.)
PC1 (32.2% explained var.)
4
2
0
-2
-5.0
-2.5
0.0
2.5

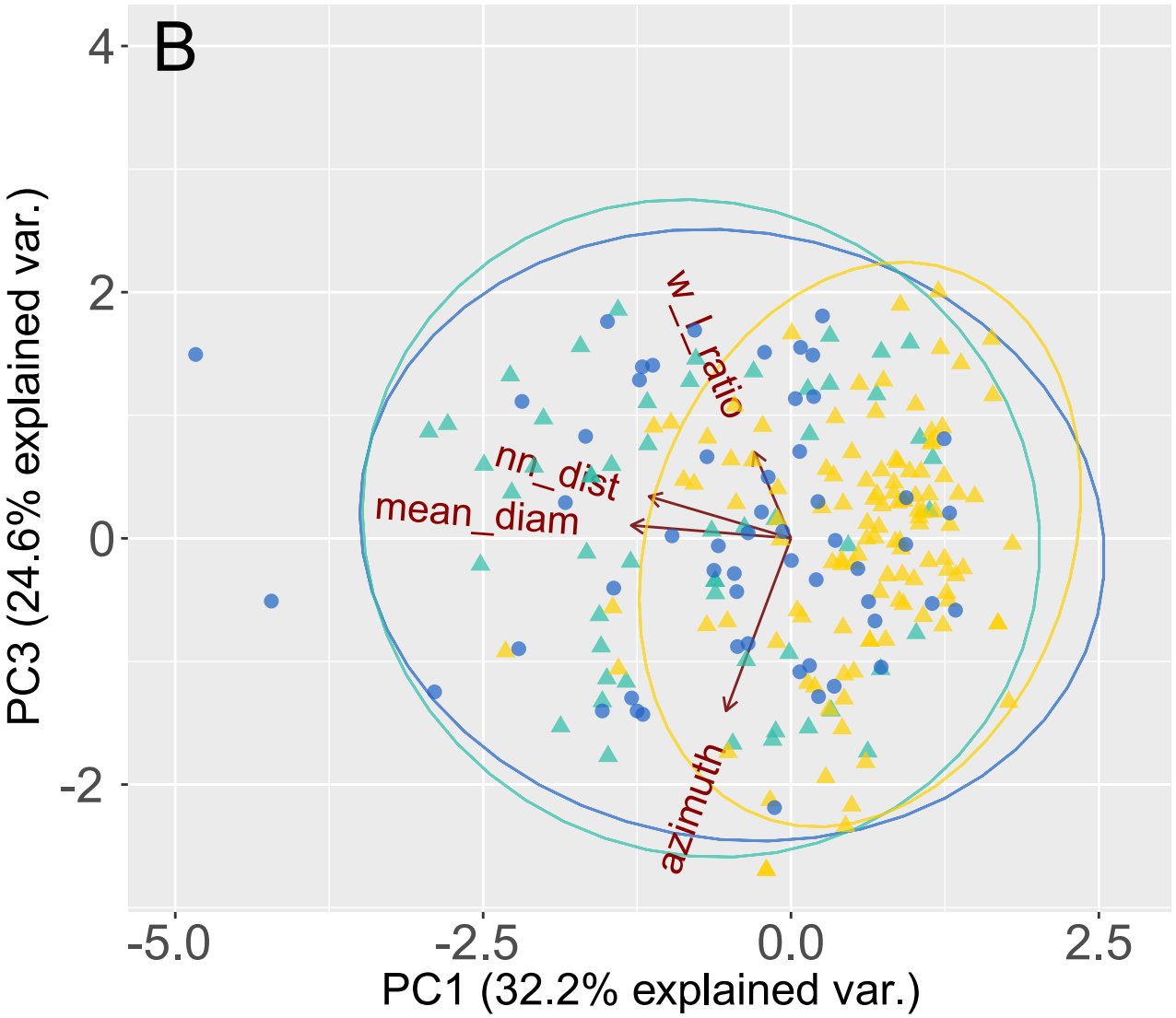
B
w_l_ratio
nn_dist
mean_diam
azimuth
PC3 (24.6% explained var.)
PC1 (32.2% explained var.)
4
2
0
-2
-5.0
-2.5
0.0
2.5

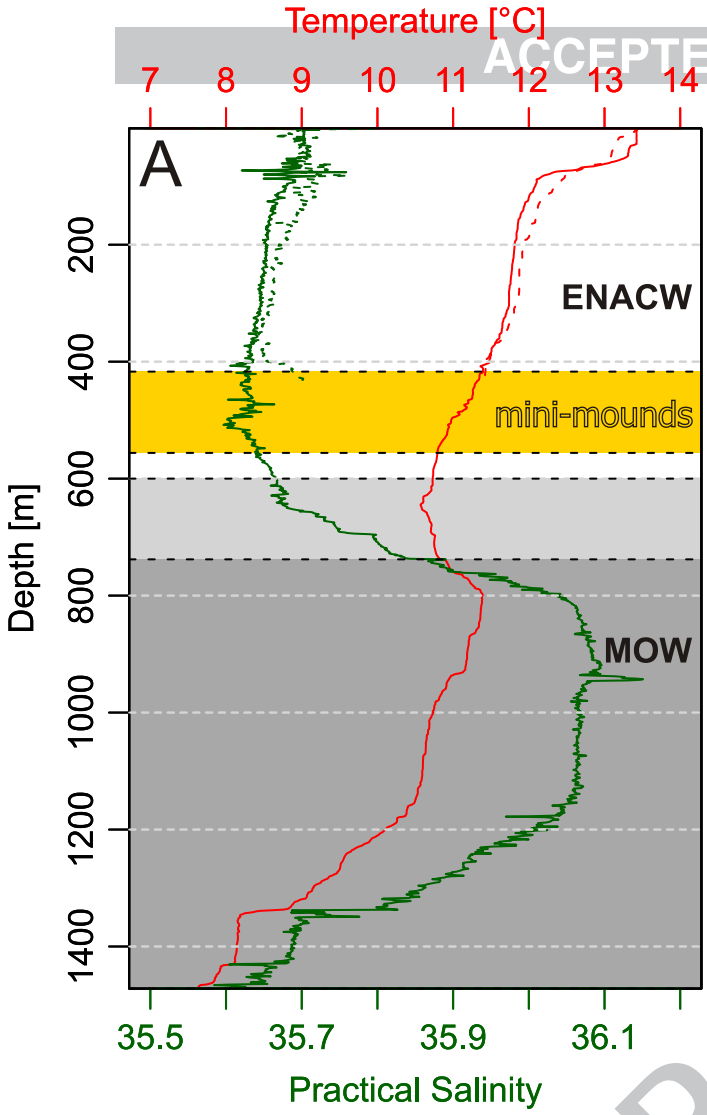

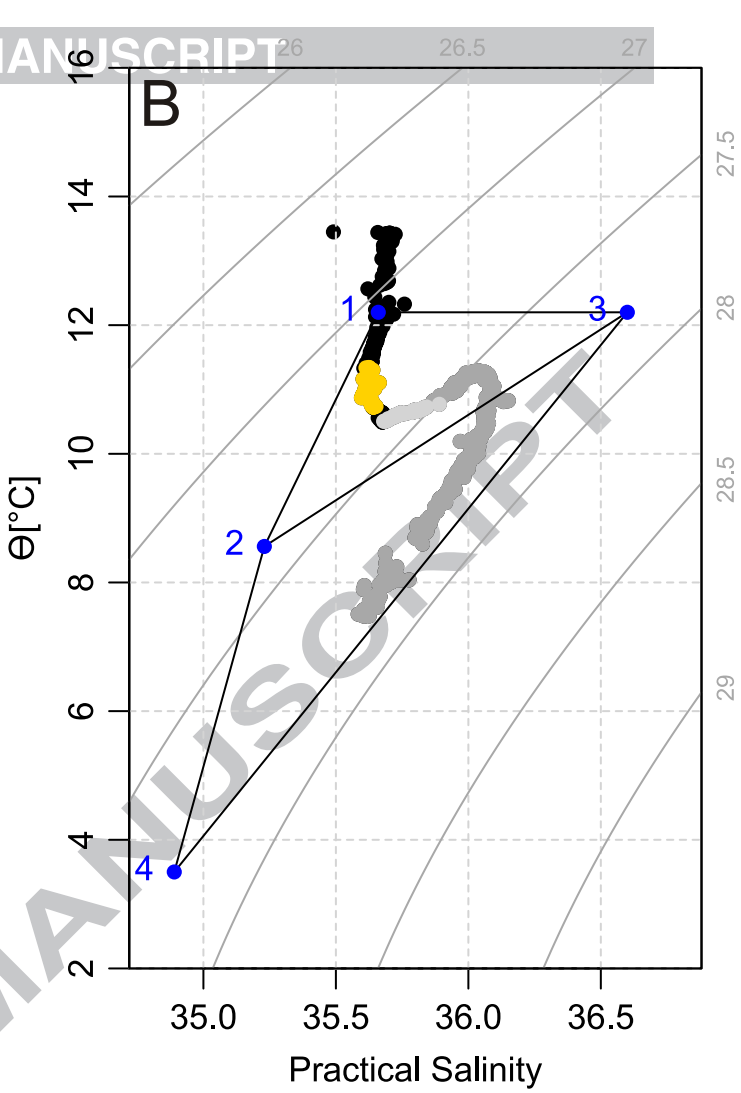

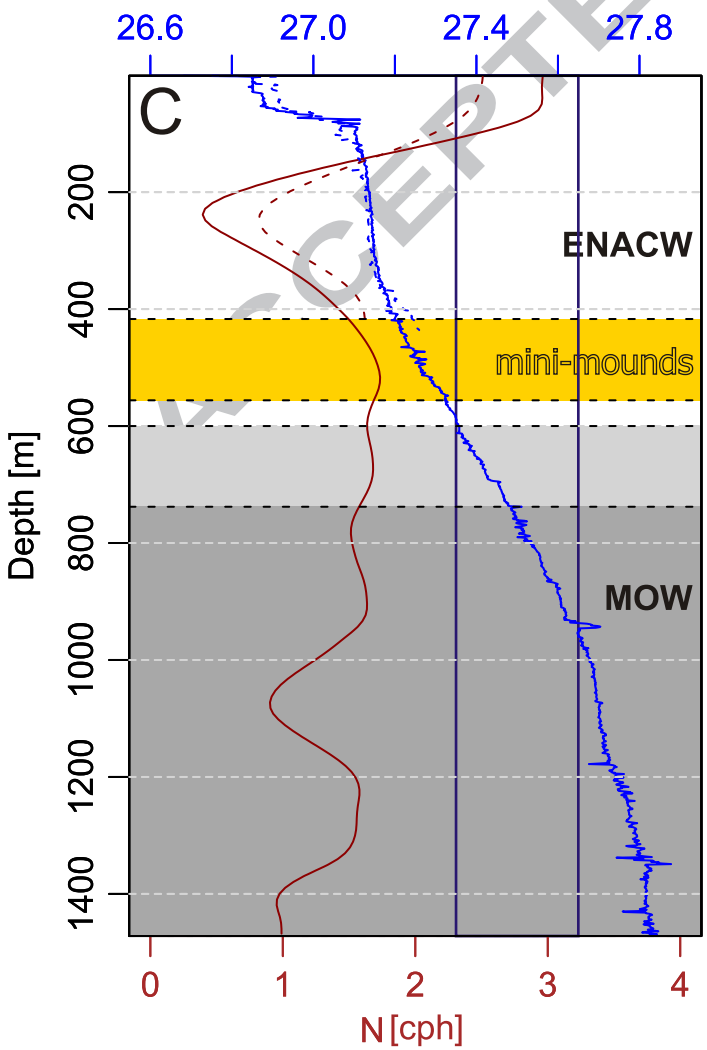

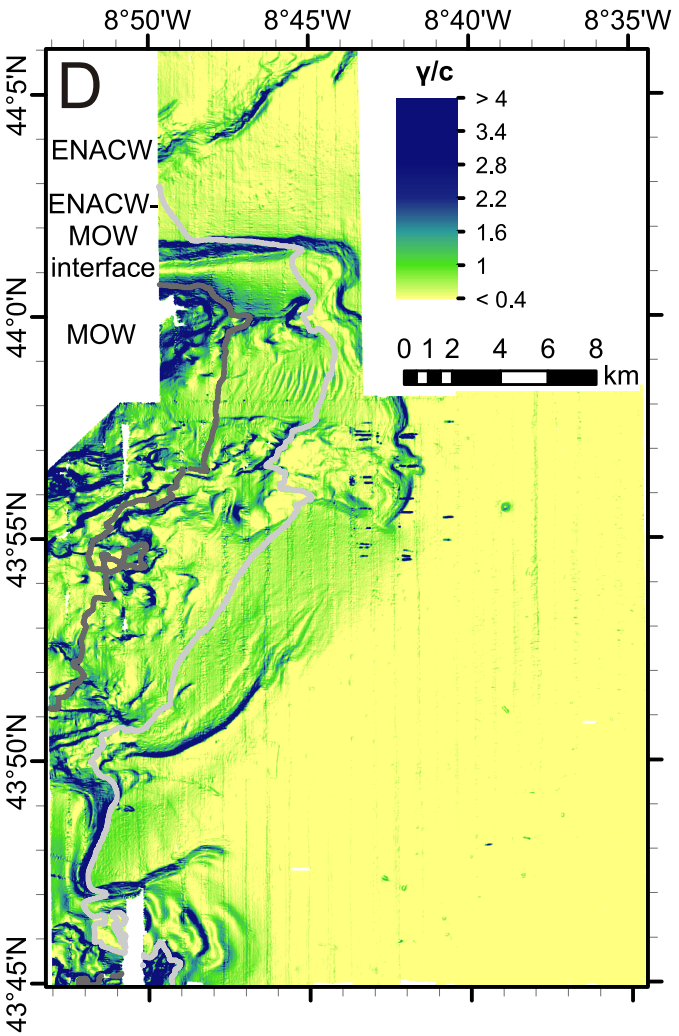

group	n	water depth m	diameter m	height/depth m	slope °	nearest neighbour m
pockmarks	55	270-443	85 [58-121]	2.05 [1.36-3.68]	4.13 [2.82-5.81]	901 [423-1169]
southern mini-mounds	54	418-534	131 [81-167]	2.24 [1.7-3.06]	3.27 [2.72-4.12]	491 [233-910]
northern mini-mounds	117	431-554	74 [53-97]	1.77 [1.16-3.08]	3.07 [2.37-3.8]	161 [108-272]

Table 1: Number of identified features, water depth range and morphological characteristics (noted as median [interquartile range]) of the different groups.

Sample ID	$[^{238}U]$ ppm	$[^{232}Th]$ ppb	$\delta^{234}U_M$ ‰ (measured)	$^{230}Th/^{238}U$ activity ratio	$^{230}Th/^{232}Th$ activity ratio	U/Th Age ka BP	$\delta^{234}U_0$ ‰ (initial)
B09-11-1	3.370 ± 0.005	0.1492 ± 0.0001	146.81 ± 0.93	0.0978 ± 0.0001	6743.4 ± 10.3	9.640 ± 0.029	150.89 ± 0.95
B09-11-2	3.450 ± 0.003	0.2480 ± 0.0001	147.13 ± 0.78	0.0950 ± 0.0001	4036.7 ± 04.9	9.338 ± 0.027	151.09 ± 0.80
B09-11-3	3.792 ± 0.004	0.3759 ± 0.0002	145.62 ± 0.86	0.0951 ± 0.0001	2928.3 ± 03.5	9.351 ± 0.032	149.55 ± 0.88

Table 2: U/Th dating results $\delta^{234}U = ([^{234}U/^{238}U]-1) \times 1000$.

Groups in PERMANOVA test	pseudo-F statistic	permutational P-value (10000 permutations)
all	52.32	0.0001
pockmarks - southern mini-mounds	5.64	0.0174
pockmarks - northern mini-mounds	117.13	0.0001
northern mini-mounds - southern mini-mounds	60.159	0.0001

Table 3: Results of PERMANOVA test for all groups and follow-up pairwise tests.

Highlights :

- Sedimentary processes in the Ferrol Canyon head are affected by bottom currents
- Bottom currents result from MOW and internal tide interaction with the canyon head
- Relict CWC mini-mounds occur upslope from favourable conditions in the canyon head
- Pockmarks provided preferential colonization surfaces for CWC mini-mound initiation
- An early Holocene shift of the ENACW-MOW interface is proposed based on CWC mini-mounds